ACRC/GCNA is an essential protease for the repair of DNA-protein crosslinks during vertebrate development

Cecile Otten[1+], Christine Supina-Pavic[1+], Marin Kutnjak[1], Ivan Anticevic[1], Vanna Medved[1], Marta Popovic[1*]

[1]Ruđer Bošković Institute, Bijenička cesta 54, 10000 Zagreb, Croatia

[+]equal contribution

[*]correspondence: mpopovic@irb.hr

Keywords

DNA repair, DNA-protein crosslinks (DPCs), ACRC/GCNA protease, zebrafish, SPRTN, histone H3, development

Summary

DNA-protein crosslinks (DPCs) are frequent DNA lesions associated with cancer, neurodegeneration and premature aging. These bulky lesions are an obstacle to all DNA transactions, but the mechanisms of DPC repair (DPCR) at the organism level are largely unknown. Because proteases play a central role in DPCR, we investigate the function of the putative protease ACRC/GCNA (ACidic Repeat Containing/Germ Cell Nuclear Antigen) which has recently been linked to DPCR, in a zebrafish model. Using a newly created fish line with a mutation in the protease core, we show for the first time that the proteolytic function of Acrc is critical for DPCR during early vertebrate development and that Acrc deficiency leads to DPC accumulation and embryonic death. We also show that Sprt domain rather than IDR domain of Acrc is essential and that Sprtn protease cannot compensate for the absence of Acrc. We identified histone H3-DPC as a novel Acrc substrate.

Introduction

Biochemical processes in cells generate by-products such as reactive oxygen species and formaldehyde, which can lead to crosslinks between DNA and proteins that are in close proximity, e.g. histones and DNA transaction enzymes. External sources of DNA-protein crosslinks (DPCs) include UV and IR radiation and various chemicals present in the environment including chemotherapeutic drugs and transition metals. Due to their bulkiness, DPCs can cause stalling of the replication and transcription machineries which can eventually lead to accumulation of mutations and/or cell death. Defective repair of DPCs can lead to aberrations during replication, resulting in genome instability, which in turn can lead to cancer or neurodegeneration. DPCs are very heterogenous, depending on the size of the protein or protein complex, on the chemical nature of the crosslink and on DNA topology near the crosslink (intact DNA, double or single

strand break). DPCs are repaired by (1) proteolysis followed by removal of the peptide remnant from the DNA backbone by the action of nucleotide excision repair (NER) or tyrosyl-DNA phosphodiesterases TDP1 and TDP2 or (2) by the action of nucleases that excise the portion of DNA to which the crosslinked protein is bound[1].

Tight regulation of protease activities is crucial and has been shown to be regulated by SUMOylation and ubiquitination of the enzymes themselves and/or their substrates[2,3]. The first dedicated DPCR protease identified was the metalloprotease Wss1 in yeast[4]. Its functional homolog in metazoans is SPRTN, whose SprT-like domain mediates its protease activity which is absolutely required for DPC repair[5–9]. Notably, SPRTN is recruited to the stalled replication fork to bypass the DPC lesion. Interestingly, the acid repeat-containing protein also known as germ cell nuclear antigen (ACRC/GCNA) also harbors a SprT-like domain and has been linked to the repair of Topo-2cc and DNMT1 DPCs, but direct evidence of its protease activity is still missing[2,10,11]. Other proteases indirectly implicated in DPCR but lacking a SprT-like domain, are FAM111A, which interacts with PCNA and plays a role in repair of Topo-1cc and trapped PARP-1[12,13], and DNA Damage Inducible 1 (DDI1) and DDI2 which interact with the proteasome and promote replication fork restart after replication stress[14–19]. The precise orchestration of DPCR factors is determined by the cellular context including cell cycle phase, cell type (germline or soma), and by the physico-chemical properties of the DPC itself. Compared to somatic cells, germ cells have a high load of topoisomerase DPCs that occur during meiosis and DPC repair is absolutely crucial in germ cells to ensure proper transmission of genetic material to the next generation[10].

Given the paucity of knowledge about DPCR on the organismal level and the role of ACRC in DPCR, we turned to zebrafish (*Danio rerio*), a well-characterized vertebrate model organism, to determine the function of Acrc *in vivo*. Previous studies have shown that ACRC/GCNA plays a role in germ cells: Gcna-1 dysfunction in *C. elegans* resulted in germline lethality while *gcna* mutants in Drosophila and zebrafish showed maternal-effect lethality due to chromosome segregation defects in oocytes[10,11]. Partial redundancy with the Sprtn homolog Wss-1 in the germ line of *C. elegans* was also demonstrated in these studies[10]. ACRC is an evolutionarily ancient protein that typically harbors four domains: an intrinsically-disordered region (IDR), a Zinc finger and an HMG box for DNA binding, and the SprT-like domain, a Zinc-metalloprotease domain with a characteristic HExxH catalytic core. Interestingly, the mouse ortholog of human ACRC consists almost entirely of the IDR, and male *Gcna* knock-out mice are sterile, suggesting an important role for the IDR domain in mouse male fertility[20]. In humans, defective DPCR proteases have been associated with cancer: mutations in *SPRTN* have been identified in patients with Ruijs-Aalfs syndrome (RJALS), who suffer from progeria and early-onset liver cancer due to genomic instability resulting from DPC accumulation[21]. In contrast, mutations in ACRC have recently been associated with spermatogenic failure and male infertility[22] and *GCNA* expression has been found to be downregulated in patients with germ cell tumors[11].

Using zebrafish as an animal model, we investigated the role of Acrc in DPC repair *in vivo*, as we found that domain organization is conserved compared with human ACRC. First, we determined gene expression levels of *acrc* in zebrafish and found that it was highly expressed in all tissues

examined, with predominant expression in testis and ovary, and that *acrc* mRNA was deposited in the eggs, similarly to *sprtn* mRNA. In comparison, *Acrc* expression in mouse was detected almost exclusively in testis. Based on a newly created zebrafish mutant line with an in-frame deletion of 4 amino acids in the catalytic core of the SprT-like domain of Acrc, we show for the first time that Acrc is indeed a functional protease with an essential role in early embryonic development. Rescue experiments performed with mRNAs encoding deletion constructs of Acrc further demonstrated the importance of a functionally intact SprT-like domain and specifically catalytic glutamate (E451), thus proving that it is the proteolytic function of Acrc that is specifically required during zebrafish embryonic development. Mouse Acrc, which lacks a SprT-like domain, could not rescue the lethality phenotype. Our results show that the inability to repair DPCs during zebrafish embryonic development results in the lethality phenotype that cannot be rescued by the Sprtn protease. RADAR assays further revealed that DPC levels are increased upon loss of Acrc and that some of these DPCs consist of histone H3, a novel target of the Acrc protease.

Results

ACRC/GCNA is a highly conserved protein with a SprT-like domain

The ACRC protein is conserved with one-to-one orthology throughout the animal kingdom (Figures 1 and S1-3). With the exception of a subset of rodents that includes the house mouse (*Mus musculus*) and the rat (*Rattus norvegicus*), all vertebrate and invertebrate orthologs have a SprT-like domain (Figures 1 and S2). This is the reason why this rodent subgroup was phylogenetically very distant from other mammalian orthologs including humans and other rodents, when the phylogenetic analysis was performed using the full-length protein sequences (Figure 1). However, when we performed phylogenetic analysis using the N-terminal domains containing Asp/Ser and Arg/Lys/Pro-rich domains, all mammalian orthologs clustered together, indicating that the rodent subgroup is evolutionarily close to other mammalian groups including rodents with a SprT-like domain (Figure S3, Table S1). Using the protein alignment of ACRC SprT-like domains, the phylogenetic tree was very similar to the analysis when the complete protein sequences were used (Figures S1 and S2). The gene environments of the human and mouse *ACRC* orthologs are quite similar and partially conserved with the gene environment of zebrafish *acrc*, although the human and mouse *ACRC* genes are located on the X chromosome, whereas zebrafish *acrc* is positioned on chromosome 14 (Figure S4). Of note, zebrafish do not have sex chromosomes, and one of the chromosome clusters that determine gender in zebrafish is located on chromosome 14[23].

The SprT-like domain in ACRC orthologs is evolutionarily conserved from invertebrates to humans (Figure 2), and the 3D Alphafold structural model shows a high degree of conservation between the SprT-like domains of humans and zebrafish. Both domains were modeled with very high or high degree of confidence (per-residue confidence score, pLDDT > 90 and 70-90, respectively) (Figure 2). The ACRC protease core comprises three α-helices and three β-sheets carrying the active site, which consists of a catalytic glutamate (E593 in human and E451 in zebrafish) and three Zn^{2+}-binding histidines (H592, H596 and H609 in human and H450, H454 and H467 in zebrafish) (Figure 2). Three β-sheets are conserved at the C-terminal end of the SprT-like domain in both species. Both proteins also share a long unstructured and intrinsically disordered region

(IDR) in the N-terminal (Figures 2 and S5). Interestingly, the human and zebrafish orthologs differ greatly in their protein charge clusters: human ACRC carries a large negative (Asp/Ser-rich) and a large positive charge cluster (Lys/Arg-rich) within the IDR region, whereas zebrafish Acrc has no significantly charged regions (Figure 2). In addition, the nature of the amino acid repeats within the IDR differs: human ACRC contains many periodic repeats spanning a large portion of the IDR, whereas zebrafish Acrc has only two short repeats (R1 and R2) (Figure 2). The Alphafold model of the C-terminal part of zebrafish Acrc predicts two α-helices with high to very high confidence, as well as intermittent structured regions (low to high confidence) within the otherwise largely disordered N-terminal part. In comparison, the human ACRC has a shorter, non-structured C-terminus and is largely disordered at the N-terminal part (Figures 2 and S5). Interestingly, when comparing the human and zebrafish protein regions outside the SprT-like domain with their mouse ortholog, we observed similar large unstructured and disordered regions, including periodic repeats, whereas the charge clusters of mouse ACRC are more similar to the human ortholog (Figures 2 and S5). In summary, our detailed analysis showed that zebrafish is an excellent model to study Acrc function because it shares many features with human Acrc, including the SprT-like domain that the mouse ortholog lacks.

Acrc is highly expressed in adult zebrafish tissues with dominant expression in gonads

We determined the mRNA expression of *Acrc* in adults and embryos and compared it with the expression of Sprtn to gain more insight into the relationship between these two DPC proteases. *Acrc* shows very high expression in the gonads, particularly in the ovaries, where it is expressed 5.6-fold more than *sprtn* (Figure 3A). In comparison, the expression of *sprtn* in the testes is very high: 9-fold higher than that of *acrc*. In all other tissues examined, including brain, liver, kidney, intestine and gill, we found moderate expression of both genes (Figure 3B).

Next, we determined the expression levels of *acrc* and *sprtn* during embryonic development in zebrafish, because DPCs need to be repaired at these crucial stages, which have high replication and transcription rates. Gene expression levels of *acrc* and *sprtn* were measured in zebrafish embryos between 1 and 72 hours post-fertilization (hpf) (Figure 3C). Both genes showed the highest expression at 1 hpf, indicating maternal mRNA deposition in the egg, as zygotic transcription only begins gradually after 2 hpf and maternal transcript levels decrease between 2 and 3 hpf[24]. Expression levels of *acrc* decline rapidly until 6 hpf and remain approximately stable until 2 days post-fertilization (dpf) before declining further. In comparison, expression levels of *sprtn* also decrease rapidly until 6 hpf, but remain stable until 3 dpf. Interestingly, *acrc* levels were at least three times higher than *sprtn* levels at all stages until 2 dpf.

To further investigate the role of the SprT-like-domain, we compared *Acrc* gene expression in adult zebrafish and mouse tissues. In both species, *acrc* is strongly expressed in the gonads; however, in zebrafish, *acrc* is more strongly expressed in the ovaries, whereas in mouse, *Acrc* is almost exclusively present in the testis (Figure 3D). This confirms the previously reported high expression in germline tissues[25]. Interestingly, *acrc* expression in the mouse is extremely low in all other tissues (at least more than 200-fold less than in the testes) (Figure 4D), which may suggest that, unlike in zebrafish, Acrc in the mouse normally has no function in non-reproductive tissues.

***Acrc* maternal mutant zebrafish strains are early embryonic lethal.**

To study DPC repair *in vivo*, we generated two zebrafish *acrc* mutant strains targeting the SprT-like domain with CrispR/Cas9 (Figures 4A and S6). Using one short guide RNA (sgRNA), we obtained the *rbi5* allele consisting of an in-frame deletion of 12 nucleotides in the putative catalytic site of the SprT-like domain of Acrc, resulting in the deletion of the catalytic glutamate E451 and the following three amino acids in the protease core including the Zn bearing Histidine H454 (ΔEMCH). Using a different sgRNA, we obtained the *rbi8* and *rbi9* alleles, which have mutations that lead to frameshifts and thus premature stop codons at the 477. and 472. amino acid positions, respectively (Figure S6). The phenotype of both types of mutant strains is embryonic lethality before 24 hpf (Figures 4 and S6). Remarkably, the phenotype of these newly created mutant lines exactly recapitulates that of the previously published alleles *zf3309* and *zf3310* described by Bhargava et al.[11]. Indeed, only embryos with homozygous mutant mothers show an early lethality phenotype, whereas homozygous mutant embryos with heterozygous mothers show no morphological defects (Figure 4B-F). The fact that the mutant strain with the catalytic mutation (rbi5, ΔEMCH) is embryonic lethal indicates that the proteolytic function of Acrc is responsible for the observed phenotype. Furthermore, we hereby confirm the requirement for maternal deposition of Acrc protein and/or mRNA in the eggs.

The putative catalytic core of the SprT-like domain is essential for Acrc function during early embryonic development.

To confirm that the catalytic mutation is responsible for the lethal phenotype and to gain insight into the function of other Acrc domains, we injected *in vitro* transcribed and capped mRNA encoding the wild-type or mutated versions of Acrc into $acrc^{rbi5/rbi5}$ maternal mutant embryos at the 1-cell stage and examined whether they could compensate for the loss of Acrc and thus "rescue" the early lethality phenotype of the *acrc* mutant. For these "rescue" experiments, we generated the following rescue plasmids encoding: full-length wild-type DrAcrc (#553, aa 1-586), full-length DrAcrc with the E415A mutation (#581), truncated DrAcrc lacking the C-terminal tail (#582, aa 1-535), truncated DrAcrc lacking the SprT-like domain (#583, aa 1-377), truncated DrAcrc lacking the R/K/P-rich domain and the SprT-like domain (#584, aa 1-269), and DrAcrc with a deletion of the internal R/K/P-rich domain (#585, aa 1-277 followed by 378-586) (Figures 5A and S7A). Each *in vitro* synthesized RNA was injected into WT and *acrc* maternal mutant embryos, and the resulting phenotypes were scored according to severity in 5 categories of overall abnormality (Figures 5B and S7B). This was performed with $acrc^{rbi5/rbi5}$ maternal mutant embryos (Figure 5, Table S2) and further confirmed in $acrc^{rbi8/rbi9}$ maternal mutants (Figure S7, Table S3). The results clearly showed that only two constructs could rescue the *acrc* mutant phenotype: the WT construct (#553) as expected, and the construct with an intact SprT-like domain but lacking the very short unstructured C-terminal tail (#582) (Figures 5B and S7B-C, Tables S2-S3): 86.8 ± 11.8% of $acrc^{rbi5/rbi5}$ maternal mutant embryos injected with WT DrAcrc were still alive after 24 hpf (92 embryos analyzed in 3 experiments), and 50% after injection with the C-terminal deletion #582 (17 embryos analyzed); for $acrc^{rbi8/rbi9}$ maternal mutants, 94.8 ± 3.4% were alive after injection with WT DrAcrc (475 embryos analyzed in 5 experiments), and 92.5 ± 11.8% were alive

after injection with the C-terminal deletion rescue construct #582 (119 embryos analyzed in 3 experiments) (Tables S2-4).

Importantly, the rescue construct encoding the full-length DrAcrc protein with the catalytic mutation E451A (#581) did not rescue the *acrc* mutant phenotype (0 ± 0% for both maternal mutants, 28 embryos analyzed in 2 experiments for *acrc*$^{rbi5/rbi5}$, 193 embryos analyzed in 4 experiments for *acrc*$^{rbi8/rbi9}$), indicating that glutamate 451 located in the protease core domain is crucial for Acrc function during early embryonic development (Figures 5B and S7B). The other constructs lacking the R/K/P-rich domain (#585) and the entire C-terminal half of Acrc (#584) also failed to rescue the *acrc* mutant phenotype, possibly due to misfolding of these truncated Acrc proteins. The construct lacking the SprT-like domain (#583) also did not rescue the *acrc* mutant phenotype, either due to the crucial role of the Sprtn-domain or to misfolding. To verify that the rescue RNAs were indeed present in the injected embryos, we collected embryos at 2 dpf and determined the expression levels of *acrc* by qRT-PCR. Total levels of *acrc* were increased (1.46- to 3.63-fold change) in embryos injected with the rescue constructs #581, 582, and 583 (Figure S8A). Since the rescue effects are observed before 1 dpf, this strongly suggests that the injected RNAs are persistently present in the injected embryos until at least 2 dpf.

Overall, the rescue experiments clearly demonstrate that Acrc is an active protease whose protease activity is absolutely required for survival at early embryonic stages. Remarkably, *acrc* maternal mutant embryos of both strains (*rbi5* and *rbi8/9*) injected with full-length WT DrAcrc reached adulthood and were fertile, allowing us to breed and maintain *acrc* mutants.

Zebrafish Sprtn and Mouse Acrc cannot compensate for loss of zebrafish *acrc* during early embryonic development.

Next, we generated a construct for the expression of DrSprtn (#603) to determine whether Sprtn could compensate for the absence of Acrc, as it is also a protease with a similar SprT-like domain (Figure 6A). Injection of DrSprtn RNA into *acrc*$^{rbi5/rbi5}$ maternal mutant embryos failed to rescue the early lethality phenotype: 0 ± 0% of injected *acrc* maternal mutants were still alive at 1 dpf (105 embryos analyzed in 2 experiments) (Figure 6B, Table S4), highlighting the unique function of Acrc during early embryonic development. Because mouse Acrc differs significantly and lacks a SprT-like domain and thus a protease activity, we injected MmAcrc RNA into zebrafish *acrc*$^{rbi5/rbi5}$ maternal mutant embryos (Figure 6A). This did not rescue the early lethality phenotype: 0 ± 0% of the injected *acrc* maternal mutants were still alive at 1 dpf (105 embryos were analyzed in 2 experiments) (Figure 6B), further confirming that Acrc protease activity is required for its function in early development, rather than the other Acrc domains. Injections of both mRNA were not toxic per se, as confirmed by injection into WT embryos: uninjected WT: 90 ± 5.3% alive at 1 dpf (n=3 experiments, 119 embryos), WT + MmAcrc (#608): 91 ± 7.9% alive at 1 dpf (n=2 experiments, 107 embryos), WT + DrSprtn (#603): 96.8 ± 2% alive at 1 dpf (n=2 experiments, 78 embryos) (Table S4). To verify that the rescue RNA was indeed present in the injected embryos, we collected embryos at 1 dpf, extracted the total RNA, reverse transcribed it, and determined the expression levels of *sprtn* (Figure S8B). The qRT-PCR results showed a 4.9-fold increase in total RNA of *sprtn* after injection of DrSprtn mRNA. Similarly, we performed RT-PCR on 2 dpf embryo samples (n = 20 embryos each) to detect MmAcrc. Indeed, because this

gene is not naturally expressed in WT zebrafish embryos, the PCR to detect MmAcrc was only successful when embryos were injected with MmAcrc RNA (Figure S8C).

Zebrafish *acrc* mutants have higher levels of DPCs, including histone H3-DPCs.

Having confirmed that the proteolytic function of Acrc is essential during early embryonic development, we investigated whether Acrc plays an active role in DPC repair *in vivo*. Therefore, we first quantified DNA-Protein crosslinks in *acrc* maternal mutants compared with WT embryos by using the SDS-KCl method to selectively precipitate stable, covalent DNA-protein complexes. The anionic detergent SDS is known to bind proteins but not DNA. Addition of KCl to an SDS solution results in the formation of an insoluble K-SDS precipitate that can be easily recovered by slow centrifugation. Protein-free DNA and protein-bound DNA are thus separated, as the free DNA remains in the supernatant, while the protein-bound DNA is precipitated. Thus, the amount of DNA in the SDS pellet is a direct measure of DNA-protein crosslinks[26]. Here, we outcrossed an *acrc*$^{rbi8/9}$ mutant female with a WT male (see Figure 4F) and collected their heterozygous progeny, all of which are "maternal *acrc* mutants", before the onset of necrosis resulting from the lack of maternally-deposited Acrc at 6 hpf. Compared with WT, the percentage of crosslinked DNA relative to free DNA in maternal *acrc* mutant embryos was increased by 78% (from 18.04 ± 3.09% to 32.75 ± 2.88%), indicating that Acrc plays a role in DPC repair at 6 hpf (Figure 7A).
For more detailed analysis, we examined DPC repair using the RADAR assay, in which DNA is precipitated from lysed tissues by ethanol and separated on an SDS-PAGE gel, and then its covalently bound adducts can be detected by silver staining and western blotting[27]. First, we examined total DPC levels by silver staining in 6 hpf embryos: *acrc*$^{rbi5/rbi5}$ homozygous maternal mutants had significantly increased levels of total cellular DPCs compared with WT embryos (Figure 7B, Figure S9A). Interestingly, the increased levels of DPCs were found in the high (>151 kDa), medium (41-150 kDa) and low (<40 kDa) molecular weight regions of the SDS PAGE (HMW, MMW, LMW), suggesting that Acrc has multiple substrates (Figure 7B, Figure S9A). For specific detection of crosslinked histone H3, we performed western blot after the RADAR assay with the same samples. The samples of *acrc* mutant embryos had significantly increased level of crosslinked histone H3 compared with WT (Figure 7C, Figure S9B).
To investigate the role of Acrc in DPCR after 2 dpf, we used *acrc*$^{rbi5/+}$ heterozygous embryos (progeny of homozygous fathers and WT mothers) because homozygous embryos die before 10 hpf. These heterozygous embryos had no obvious phenotype and are viable and fertile. To test their ability to repair DPCs, we treated them with 10 mM formaldehyde (FA) for 30 minutes, which normally induces DPCs. As seen on the silver gels, heterozygotes did not show significantly increased DPC levels compared with WT, either untreated or after treatment with FA. However, as expected, treatment with FA itself significantly increased DPC levels in both WT and heterozygotes (Supplemental Figure S10). Remarkably, endogenous histone H3-DPC levels were increased in heterozygotes compared with WT, although the change was not statistically significant (Supplemental Figure S11A). In a complementary experiment, we incrossed heterozygous *acrc*$^{rbi5/+}$ males and females, and their progeny of mixed genotypes (WT, heterozygotes and mutants) was collected at 3 dpf, as they were all viable thanks to maternally deposited Acrc. Using the SDS-KCl method described above, we analyzed total DPC levels in those embryos treated for 1 hour with a low dose of FA (5 mM). Treatment of WT embryos with FA did

not result in significant changes in DPC levels (3.12 ± 0.29% to 2.79 ± 0.14% in WT + FA). However, the *acrc*$^{rbi5/+}$ progeny showed more than twofold increased DPC levels after treatment with FA (3.09 ± 0.26% to 7.08 ± 1.40%) (Supplemental Figure S11B). These results suggest that embryos with reduced Acrc levels are more sensitive to FA-induced DPCs, further confirming the role of Acrc in DPC repair.

Discussion

We report that the Acrc protein is essential during vertebrate embryonic development through its function as a DPC repair protease. A functional SprT-like domain, and, in particular, a catalytic glutamate, are indispensable for the full functionality of Acrc and thus for embryo survival. Our *in vivo* analysis of different Acrc domains showed that the SprtT-like domain is required to rescue the lethality phenotype in *acrc* mutants, while the intrinsically disordered region (IDR) alone is not sufficient. We show that Acrc plays a specific role in DPCR during early embryonic development, that is distinct from that of Sprtn. We identified histone H3-DPC as one of the Acrc substrates in zebrafish embryos.

Given its essential function during vertebrate embryonic development, it is not surprising that ACRC is highly conserved throughout the animal kingdom and exhibits one-to-one orthology (Figures 1 and S1-3). In support of our functional studies, we found that the SprT-like domain in the C-terminal half of ACRC is remarkably conserved from invertebrates to human (Figures 1 and S2), while the N-half of the protein is largely disordered and variable across species (Figure S3). Considering that the mouse ACRC lacks a SprT-like domain[25], we performed an in-depth analysis of rodent ACRC orthologs and showed that many rodent species possess a SprT-like domain; it will be interesting to determine why it has been lost during evolution specifically in certain mouse and rat species (Figures 1 and S1-3). We have also shown that the 3D structural model of the SprT-like domain of the human and zebrafish ACRC orthologs is nearly identical (Figure 2), making zebrafish an excellent model for studying ACRC-mediated DPC proteolysis.

ACRC was originally described as a protein with a specific role in germ cells[10,11,25], while a recent study suggests an important role in somatic cells of *C. elegans*[2]. We therefore investigated mRNA expression of *acrc* in adult zebrafish tissues. We found very high and dominant expression of *acrc* in both ovaries and testes (Figure 3A) consistent with previous work showing that Acrc plays an important role in germ cells[10,11,20]. Interestingly, we found that *acrc* is expressed in all other tissues analyzed (Figure 3A). In contrast, we confirmed that mouse *Acrc* is expressed almost exclusively in the testis (see Gene Expression Database for Gcna under www.informatics.jax.org, February, 2023, and Figure 3C) which further highlights the difference between mouse Acrc which lacks a SprT-like domain and other vertebrate orthologs (Figure 2). Of note, *ACRC* gene expression patterns in humans are more similar to zebrafish *acrc* expression patterns, since human *ACRC* is expressed in adult somatic tissues[28]. Considering the substantial mRNA expression levels of *acrc* in adult tissues of zebrafish and humans, we suggest it also plays a role beyond DPC repair in meiosis in the germline.

Comparison of the expression levels of *acrc* and *sprtn* during zebrafish embryonic development showed that both genes are highly expressed up to 6 hpf, but also that *acrc* is expressed at least

three-fold more strongly between 1 hpf and 48 hpf, suggesting that Acrc is the dominant DPCR protease at these stages (Figure 3D). This is supported by our results showing that Acrc is absolutely required during embryonic development (Figure 4C).

We showed that the proteolytic function of ACRC is essential for embryonic survival, as the transgenic line with the deletion of the catalytic glutamate (E451) and three downstream amino acids (*rbi5* allele, Figure 4) resulted in embryonic death after 6 hpf (Figure 4C). Previously, it was observed that the absence of the entire ACRC protein is lethal in zebrafish[11], but it was not known which domains of the ACRC are responsible for this phenotype. Considering that ACRC mutants fully recover after injection of ACRC WT mRNA into embryos at the one-cell stage and reach adulthood without obvious defects, we suggest that ACRC is the only DPCR factor that can repair specific DPC lesions at the early developmental stages. Other DPC proteases or nucleolytic DPC repair pathways cannot compensate for the loss of ACRC activity at this stage. Thus, we conclude that the function of Acrc in the soma during development is essential for embryo survival. In contrast, Acrc is not essential in adults, as rescued *acrc* mutants develop normally.

Our flexible non-genetic rescue system allows us to rapidly test different constructs encoding mutant forms or deletions of Acrc in a vertebrate model organism. Here, we used this system for the first time to examine the function of individual domains of Acrc. First, we confirmed the specificity of the results from the *rbi5* mutant transgenic line that the catalytic function of Acrc is essential, because injection of *acrc* mRNA with the E451A mutation did not rescue the lethality phenotype (Figures 4, 5, S6, S7). Previously, a similar experiment was performed in *Drosophila* using transgenic expression of WT and HE>AA mutant Acrc/Gcna in the mutant background[11] which showed that dsDNA breaks were not rescued by the HE>AA mutant, while egg hatching impairment was rescued, thereby indicating a separate function for Acrc/Gcna besides its catalytic activity. Using this separation-of-function method, we found that deletion of the SprT-like domain impairs the function of Acrc and that the IDR domain alone cannot rescue the lethality phenotype (Figure 5), confirming that the proteolytic function of ACRC and not the IDR domain is essential for development. We additionally confirmed these findings by injecting mouse Acrc mRNA which consists only of the IDR region (Figure 2). Interestingly, an ACRC conditional KO mouse model showed defects in spermatogenesis including dsDNA breaks and defective chromatin compaction, possibly via the TOP2 interaction, but a direct role of mouse Acrc in DPCR has not yet been identified. Instead, it has been proposed that mouse Acrc promotes genome integrity during meiosis by mediating protein-protein interactions via its IDR domain and its SUMO-interaction motifs[10] and by acting as a histone chaperone[29].

We show that Sprtn and Acrc are not redundant, considering that *sprtn* is endogenously expressed during the onset of lethality in ACRC mutants and the fact that injection of *sprtn* mRNA (Figure 3D) could not compensate for the lethality phenotype (Figure 6). Our results are consistent with previous observations from genetic experiments *in C. elegans* that showed that these two DPC proteases work in parallel pathways[2,10].Previously, Acrc was shown to be involved in the elimination of formaldehyde-induced DPCs in *C. elegans*[2], and DPCs were found to accumulate in zebrafish and *Drosophila acrc* mutants[11]. Because a catalytic mutation in the protease core causes early embryonic lethality, we investigated whether DPC accumulation

precedes the lethality phenotype. Indeed, endogenous DPC levels are significantly increased in mutant embryos at 6 hpf before the onset of lethality (Figure 7A), suggesting a link between DPCR and the phenotype. Because the increase in total DPC levels, although significant, was not very high, we investigated whether specific DPCs accumulate. Indeed, we identified a very high accumulation of histone H3-DPCs in *acrc* loss-of-function embryos, demonstrating for the first time that H3 is a substrate for the Acrc protease and that Acrc is involved in histone DPC repair during vertebrate development. So far, only Sprtn was shown to cleave H3, while a direct role of Acrc and of the Ddi1 protease in H3-DPC removal has been suggested[6,30]. Considering that H3 is a known SPRTN substrate[6] and that zebrafish Sprtn fails to rescue the *acrc* mutant phenotype (Figure 6), we deduce that the accumulation of H3-DPCs is most likely not the cause of embryonic lethality in the mutants. In the total DPC analyses, we saw increased levels of several low, medium, and high molecular weight DPCs, suggesting that Acrc proteolyzes many DPC substrates during development that apparently cannot be repaired by Sprtn. It remains to be elucidated which are Acrc-specific DPC substrates that cause the lethality phenotype in zebrafish when accumulated. One possibility is DNMT1, which methylates newly replicated DNA strands and is suggested to be an Acrc substrate in *C. elegans*[2]. Top2 is another candidate, as RADAR assays followed by mass spectrometry revealed that the topoisomerase Top2 forms DPCs in *Drosophila gcna* mutants. Moreover, TOP2 is known to be abundant in the germline and to have germline-specific functions, as well as to be necessary for paternal chromatin remodelling and zygotic genome activation (ZGA)[10]. However, Top2 is also a substrate of Sprtn[6], and possibly other proteases. In adult tissues, a possible substrate is Spo11, which creates DNA breaks during meiosis and is a primary DPC substrate during oogenesis in *Drosophila*[11]. Furthermore, mass spectrometry data from Larsen et al. (2019)[3] showed that both ACRC and SPRTN are recruited to a DPC lesion in replication dependent manner, suggesting that both proteases act within a similar time frame in cells. Taken together, our experiments confirm that Acrc and Sprtn share some common targets but act in parallel pathways.

Cellular processes change tremendously during embryonic development: in zebrafish, the fertilized egg initially develops using maternally deposited mRNAs and proteins until the Maternal-Zygotic Transition (MZT) occurs around 3 – 4 hpf, leading to zygotic genome activation (ZGA)[31]. Additionally, during this time, cells divide every 30 minutes, which means that many DNA transactions occur simultaneously, such as DNA unwinding, transcription, replication and heterochromatin formation, which in turn makes DNA highly susceptible to DPC formation. Since this is a crucial time during vertebrate embryonic development, fidelity of DNA repair is absolutely essential. In conclusion, it remains to be clarified which are the relevant DPCs that can be specifically repaired by the Acrc protease in embryonic development.

Acknowledgments

Mouse tissues were a kind gift from Prof. Tihomir Balog, Ruder Boskovic Institute (RBI). The pCS2+HisMyc plasmid used for cloning the rescue constructs was a kind gift from Prof. Salim Seyfried, Potsdam University, Germany. The M.P. research group is supported by the Croatian

Science Foundation Installation Grant (UIP-2017-05-5258), the Slovenian-Croatian Bilateral Research Project grant (IPS-2020-01-4225) and the European Structural and Investment Funds STIM – REI project (KK.01.1.1.01.0003).

Author contributions

CS-P, CO and MK created the transgenic zebrafish lines. MP performed the phylogenetic and structural analysis. CS-P and VM performed the expression experiments. CO performed the rescue experiments. MK and IA performed the DPC analyses. CO and MP wrote the manuscript. MP designed and supervised the project.

Declaration of interests

The authors declare that they have no conflict of interest.

Figure titles and legends

Figure 1. Phylogenetic analysis of ACRC/GCNA orthologs. Full-length protein sequences were aligned using MAFFT and the phylogenetic tree was constructed in PhyML. Blue: non-rodent mammals, dark blue: rodents and bats with a SprT-like domain, grey: rodents without SprT-like domain, green: birds, red: reptiles, yellow: amphibians, orange: fish, colorless: invertebrates.

Figure 2. Comparison of human, zebrafish and mouse ACRC/GCNA protein domains and motifs and structural model of human ACRC**.** Domains and motifs were identified using SAPS and Motif Scan workspace. Models were build using Alphafold and analyzed with Chimera. HEXXH, protease core; IDR, Intrinsically Disordered Region; R, repeats. The metalloprotease core of ACRC includes the active glutamate shown in red and Zn^{2+} binding histidines shown in orange.

Figure 3. Expression patterns of *acrc* in comparison with *sprtn* quantified by qRT-PCR. A, B - Expression levels of *acrc* (A) and *sprtn* (B) in tissues of adult zebrafish. The only significant change in gene expression for *acrc* between male and female was in kidneys and gonads. C - Expression levels of *Acrc* in tissues of adult mice. The only significant change in gene expression for *Acrc* between male and female was in gonads. D - Comparison of *acrc* and *sprtn* expression levels in zebrafish embryos at 1, 4, 6, 12, 24, 48 and 72 hpf. The only significant change in gene expression was between 1 and 6 hpf for *acrc.* Data represent MNE (Mean Normalized Expression) ± S.E.M. normalized to the housekeeping genes *elongation factor 1α (eef1a1l1*) for zebrafish and *Rplp0* for mouse. F = female; M = male.

Figure 4. Creation of two *acrc* mutant zebrafish strains. A - Scheme of the Acrc protein and the position of the 4 amino-acids deletion (Δ-EMCH, aa 451-454) in the enzymatic core of the SprT-like domain in the *rbi5* allele, which was created using CrispR/Cas9 technology. B, C – representative pictures of 1 dpf embryos: WT (B) and *acrc* maternal mutants (C). D-F: schemes representing the genotype-phenotype correlations upon loss of one or both *acrc* WT alleles. D – crossing a WT female with any male (WT - white, heterozygote - stripes or mutant - grey) always leads to viable fish since heterozygous embryos are viable; E - crossing a heterozygous female with any male (WT, heterozygote or mutant) always leads to viable fish: Acrc is normally deposited in the egg and therefore even mutant embryos are viable; F - crossing an *acrc* mutant female with any male (WT, heterozygote or mutant) always results in embryos with an early lethal phenotype (black yolk), henceforth called „*acrc* phenotype", due to lack of Acrc deposition

in the egg, irrespective of the genotype of the embryo itself (mutant or heterozygote); these embryos are henceforth called „maternal *acrc* mutants".

Figure 5. WT Acrc mRNA injections fully rescue the *acrc* maternal mutant phenotype. A – scheme of the injected rescue constructs: #553: DrAcrc-WT, #581: DrAcrc-E451A, #582: DrAcrc-ΔCterm, #583: DrAcrc-ΔSprtn, #584: DrAcrc-IDR, #585: DrAcrc-ΔR/K/P. B – phenotype characterization of rescued embryos with representative pictures. WT and *acrc*$^{rbi5/rbi5}$ maternal mutant embryos were injected with 1nl of 250ng/µl RNA derived from the rescue constructs described above. Phenotypes were scored at 1 dpf and divided into 5 categories: #1: dead, #2: necrotic, #3: very abnormal, #4: abnormal, #5: WT-like. Embryos in categories #3, 4 and 5 were considered alive. For detailed results, see Supplemental Table 1. Data shown are means

Figure 6. DrSprtn and MmAcrc mRNA injections do not rescue the *acrc* mutant phenotype. A – scheme of the injected rescue constructs: #608: MmAcrc, #603: DrSprtn. B – phenotype characterization of rescued embryos with representative pictures. WT and *acrc*$^{rbi5/rbi5}$ maternal mutant embryos were injected with 1nl of 250ng/µl RNA derived from the rescue constructs described above. Phenotypes were scored at 1 dpf and divided into 5 categories: #1: dead, #2: necrotic, #3: very abnormal, #4: abnormal, #5: WT-like. Embryos in categories #3, 4 and 5 were considered alive. For detailed results, see Supplemental Table 4. Data shown are means

Figure 7. DPC measurements in 6 hpf zebrafish acrc mutant embryos. A – Total DPC levels (percentage of DNA-protein crosslinks vs. free DNA) as quantified using the KCl/SDS method: increased DPC levels in acrcrbi8/9 maternal mutants relative to WT. An unpaired Student's t-test was performed for 3 biological replicates, pools of 100 embryos each (***: p-value = 0.0254). B-C – RADAR assays on 6 hpf embryos. Unpaired Student's t-test were performed for 4 biological replicates, pools of 50 embryos each (****: p-value < 0.0001). B – Total DPCs were isolated from n = 50 embryos each for WT and acrcrbi5/rbi5 homozygotes, resolved on an SDS acrylamide gel, and stained with silver. Dot-blots showing DNA loading controls for DPC analysis prior to benzonase treatment are shown below; a DPC equivalent of 50 ng total DNA was loaded per well. C – Quantifications of total DPC staining intensities normalized to WT (top), and of staining intensities for high, middle and low molecular weight DPCs (bottom) based on data shown here and in Supplemental Figure S9A (4 biological replicates). D – Histone H3-DPC detection by western blot, with corresponding dot blot for dsDNA as loading control; a DPC equivalent of 50 ng total DNA was loaded per well. Total DPCs were isolated from 6-hpf old embryos, separated by SDS-PAGE and detected with histone H3-specific antibody. Quantification normalized to WT based on data shown here and in Supplemental Figure S9B (5 biological replicates). An unpaired Student's t-test was performed for 3 biological replicates, pools of 50 embryos each (****: p-value < 0.0001). L = ladder. Data shown are means with S.E.M.

Tables with titles and legends

Materials and Methods

Phylogeny and syntenic analysis

Nucleotide and protein sequences were retrieved from the NCBI (http://www.ncbi.nlm.nih.gov/) database using Blastx algorithm. Sequences were aligned with MUSCLE algorithm[32] and phylogenetic tree was constructed using Maximum Likelihood method in PhyML 3.0.1 software[33]. Orthology predictions using conserved synteny analysis between zebrafish and humans for genes of interest were made using Genomicus (http://www.genomicus.biologie.ens.fr/genomicus), a conserved synteny browser synchronized with genomes from the Ensembl database[34].

Model prediction

Domains and motifs were identified using SAPS and Motif Scan workspace[35–37]. Protein topology schematics was visualized using IBS software[38]. Models were build using Alphafold[39,40] and analyzed and visualized with UCSF Chimera[41]. Disorder probability was predicted using PONDR-FIT[42].

Zebrafish lines and handling

Adult wild-type (WT) zebrafish of the AB strain are kept at 28.5°C on a 14-hour light and 10-hour dark cycle under standard conditions. Originally, adult zebrafish of both sexes of the AB strain were obtained from the European Zebrafish Resource Center at the Karlsruhe Institute of Technology (Germany). Zebrafish embryos were collected and kept in E3 medium (5mM NaCl; 0.17mM KCl; 0.33mM $MgSO_4$; 0.33mM $CaCl_2$) in Petri dishes at 28.5°C until 3 dpf under standard conditions. All handling and experiments were performed in accordance with the directions given in the EU Guide for the Care and Use of Laboratory Animals, Council Directive (86/609/EEC), and the Croatian Federal Act on the Protection of Animals (NN 135/2006).

Pharmacological treatment

For DPC induction, 3 dpf zebrafish embryos were maintained at 28.5°C and incubated in 5 mM formaldehyde in E3 medium for 1 hour for the SDS-KCl measurements, and in 10 mM formaldehyde for 30 minutes for the RADAR assays of 2 dpf embryos as described below.

Microinjections

Microinjections were performed using a microinjection system (Laboratory microinjector – FemtoJet® 4x series – Eppendorf) and needles (Eppendorf™ Femtotips™ Microinjection Capillary Tips). Microinjections in 1- to 4-cell stage embryos were performed by injecting 1 nl of premixed solutions into the yolk for the following purposes: 1) creating zebrafish *acrc* mutant lines using the CrispR/Cas9 system, 2) rescue of the *acrc* mutant phenotype by mRNA injection. Embryos were then maintained in E3 medium under standard conditions at 28.5°C and staged as previously described[43].

Creation of mutant zebrafish strains using CRISPR/Cas9 system, genotyping

Genetically modified zebrafish lines were created using Cas9 protein (EnGen® Spy Cas9 NLS, #M0646T, NEB) and previously established protocols combining PCR and reverse transcription to generate guide RNAs[44]. To create specific zebrafish *acrc* mutant strains, the following two guides targeting *acrc* exon 12 were designed using the CRISPRscan software (http://www.crisprscan.org/):

DrACRC sgRNA 1	5'-GGAGCATAAAGCCTCCAGAA-3'	Resulting mutations: *rbi8, 9*

DrACRC sgRNA 2	5'-GGCCGCATGACACATTTCA-3'	Resulting mutation: *rbi5*

To introduce *acrc* mutations in exon 12, 1-cell stage zebrafish embryos were microinjected with 1 nl of the following solution: guide RNA (180 ng/µL), Cas9 protein (600 ng/µL), and KCl (300 mM). F0 injected embryos were raised and founders were later identified by sequencing of F1 progeny. For genotyping experiments, injected embryos were lysed with 0.5 mg/ml proteinase K (#J63710, AlphaAesar) in digestion buffer (10 mM Tris-HCl pH 8.5, 50 mM KCl, 0.3% Tween-20) for 3 hours at 55°C. PCR and sequencing was then performed using the following primer pair:

Geno_acrc_F	5'-ACAGATCGGTTACGGGATAC-3'
Geno_acrc_R	5'-TTGATGTCATAACTGTGGCA-3'

Three alleles were selected for further maintenance. All experiments were conducted with the *rbi5* allele which lacks 4 amino acids in the catalytic site of the SprT-like domain of Acrc (ΔEMCH 451-454). The mutant embryos with the other alleles (*rbi8* and *rbi9*, with 1 nte indel and 11 nte indel creating a premature stop at aa 477 and aa 472, respectively, see Supplemental Figure S6) displayed the same phenotype as *rbi5*, as well as that of the previously published alleles *gcna zf3309* and *gcna zf3310* thereby confirming the validity of the observed phenotype[11].

Rescue experiments: cloning and mRNA *in vitro* transcription

To perform rescue experiments, the WT coding sequence of zebrafish *gcna/acrc* (ENSDART00000169970.2) was amplified by PCR and cloned into the multicloning site of the pCS2+HisMyc vector[45] between the XhoI and XbaI restriction sites and verified by sequencing. The vector contains an SP6 promoter, a multicloning site, a polyA tail and a unique restriction site after the polyA tag (KpnI). RNA was synthesized using purified, linearized plasmid by performing an *in vitro* transcription with SP6 using the Hiscribe SP6 RNA kit (#E2070S, NEB) and a cap analog from the ARCA kit (#S1411, NEB) for improved mRNA stability. The resulting RNA was purified using the RNA cleanup kit (#T2040, NEB) and injected into 1-2 cell stage *gcna/acrc* maternal mutant embryos or into control WT embryos (1nl of the mRNA solution: 250ng/µl RNA in 0.3M KCl and 0.015% phenol red). In order to determine functionally relevant amino acids and domains of *gcna/acrc*, we cloned deletion constructs by inverse PCR based on the original pCS2+HisMyc-DrAcrc plasmid using the following primer pairs (see Table). RNAs were then *in vitro* synthesized and injected as described above for WT *gcna/acrc*. Similarly, we obtained rescue constructs based on the same pCS2+HisMyc vector backbone with full-length coding sequences inserted between the XhoI and XbaI restriction sites for mouse *Acrc/Gcna* (NM_001382234) or zebrafish *sprtn* (ENSDART00000158057.2) from Genosphere.

#553 pCS2+HisMyc-DrAcrc (WT)	DrAcrc_F	5'-AGAGGATCTGCTCGAGATGGATCCTGGTACTTTATCACT-3'
	DrAcrc_R	5'-TCACTATAGTTCTAGATCAACTTTGACTGAGACGAGTCT-3'
#581 pCS2+HisMyc-DrAcrc-E541A	DrAcrc-E451Amut_F	5'-GCTATGTGTCATGCGGCC-3'
	DrAcrc-E451Amut_R	5'-ATGGATTAAAGTATCCCGTAACC-3'
#582 pCS2+HisMyc-DrAcrc-Δ-Cterm	DrAcrc-Cterm-del_F	5'-TGATCTAGAACTATAGTGAGTCGTA-3'
	DrAcrc-Cterm-del_R	5'-CAACAAAACCAGCTGTCC-3'

#583 pCS2+HisMyc-DrAcrc-Δ-Sprtn	DrAcrc-Cterm-del_F	5'-TGATCTAGAACTATAGTGAGTCGTA-3'
	DrAcrc-Sprtn-del_R	5'-TTTGTTCTGTTTGAAACTCCG-3'
#584 pCS2+HisMyc-DrAcrc-IDR	DrAcrc-Cterm-del_F	5'-TGATCTAGAACTATAGTGAGTCGTA-3'
	DrAcrc-IDR_R	5'-CTGGAACTCTTCCTCGG-3'
#585 pCS2+HisMyc-DrAcrc-Δ-R/K/P	DrAcrc-R/K/P-del_F	5'-GACGAACTCACCAGCAAAC-3'
	DrAcrc-R/K/P-del_R	5'-CCTGACTCTGTCCAATAATGAC-3'

Analysis of rescue experiments

To assess rescue efficiencies, the morphology of 1 dpf non-injected and injected embryos was assessed and embryos were categorized as follows: #1: "dead"; #2: "necrotic": the yolk is intact, but the embryo is completely necrotic; #3: "very abnormal": the embryo has a very short body axis due to necrosis and incomplete embryonic development; #4: "abnormal": the embryo has a head and an elongated tail but can display defects such as cyclopia, which are typically the result of earlier necrosis; #5: "WT-like": the embryo has a morphology indistinguishable from WT. Rescue constructs were injected in at least 2 clutches, and at least n=50 embryos were categorized.

RT-qPCR to verify the presence of the rescue constructs

To verify that the rescue RNAs are present in the injected embryos, pools of 5-20 embryos were collected at 1 or 2 dpf, total RNA was extracted using the Total RNA isolation kit (#T2010, NEB) following manufacturer's instructions. Total RNA was then quantified using the Bio-Spec Nano Spectrophotometer and RNA integrity was determined by agarose gel electrophoresis. For each sample, purified total RNA was reverse transcribed using the ProtoScript II First Strand cDNA Synthesis Kit (#E6560, NEB) and a 1:1 mix of oligodT and random hexamer primers to obtain cDNA. Quantification of zebrafish gene expression was performed using the qPCR method of relative quantification in technical triplicates on 5 ng cDNA per reaction using the following primers:

DrSprtn	Primer efficiency: 96%	DrSprtn_qPCR_F (#2064)	5'-AATGACAAGTTCTTCTGGGGG-3'
		DrSprtn_qPCR_R (#2065)	5'-AAACACCAGCACATAGCGTCA-3'
DrAcrc	Primer efficiency: 86%	DrAcrcAll_qPCR_F2 (#2409)	5'- AGAACCGGTCTCAAGAGGAA-3'
		DrAcrcAll_qPCR_R2 (#2410)	5'- CTCATAGACTGCGGTTGGAC -3'
DrAtp50	N/A	DrAtp5po_qPCR_F (#2234)	5'-CTTGCAGAGCTGAAAGTGGC-3'
		DrAtp5po_qPCR_R (#2235)	5'-ACCACCAAGGATTGAGGCAT-3'
Dr18S	Primer efficiency: 83%	Dr18S_qPCR_F (#634)	5'-CGCGAGATGGAGCAATAACA-3'
		Dr18S_qPCR_R (#635)	5'-AGGGTAGGCACACGTTGAT-3'
MmAcrc	N/A	MmAcrc_qPCR_F	5'-AAAGGCTAGCTGTGTCGTGA-3'
		MmAcrc_qPCR_R	5'-TGTCAGAAGTCTCATCTCCACTG-3'

Microscopy

Zebrafish embryos were imaged using a Samsung 13-megapixel camera with an f/1.9 aperture applied to the ocular of a Motic SMZ-171 binocular.

Zebrafish and mouse tissues collection

Adult male and female zebrafish were sacrificed for tissue collection according to regulations by immersion in ice-cold water supplied with 10% MS-222 (Tricaine) for 30 min and dissected to collect the following tissues: brain, liver, kidney, intestine, gonads (testes and ovaries), eye, gills, muscle. Tissues from n= 3 adults were pooled, put in RNALater and frozen. Wild-type zebrafish embryo samples were collected and dry-frozen at 1, 4, 6, 12, 24, 48, and 72 hpf: 3 pools of 30 embryos per condition. The following mouse tissues were donated by Prof. Balog (RBI, see acknowledgments): brain, liver, kidney, intestine, gonads (testes and ovaries), and processed similarly to the zebrafish tissues. The mouse tissues were derived from 2 females and 2 males, all of them 4 months old.

RNA extraction and cDNA synthesis

Collected adult zebrafish and mouse tissue samples were thawed on ice and submitted to homogenization at 13500 min^{-1} for 30 seconds with Ultra turrax t25. Total RNA was then extracted from max. 50 μg tissue for each sample using the Total RNA isolation kit (#T2010, NEB) following manufacturer's instructions. Total RNA was then quantified using the Bio-Spec Nano Spectrophotometer and RNA integrity was determined by agarose gel electrophoresis. For each sample, 1 μg of purified total RNA was reverse transcribed using the ProtoScript II First Strand cDNA Synthesis Kit (#E6560, NEB) and random hexamer primers to obtain 50ng/μl cDNAs.

Quantitative RT-PCRs, primers

Quantification of zebrafish gene expression was performed using the qPCR method of relative quantification in technical triplicates on 10 ng cDNA per reaction using the following primers:

DrSprtn	Primer efficiency: 90%	DrSprtn_qPCR_F (#1266)	5'-ATTCCCTTCAGTGGCAGAGG-3'
		DrSprtn_qPCR_R (#1267)	5'-GAGGTTCTGGTGGCGCTTTA-3'
DrAcrc	Primer efficiency: 90%	DrAcrc_qPCR_F (#1264)	5'-ACCCAAACCACAACGTCCTT-3'
		DrAcrc_qPCR_R (#1265)	5'-ACTGGCGTGTGGATTACAGG-3'
DrEf1a	Primer efficiency: 91%	DrEF1a_F2 (#2082)	5'-TGATGCCCTTGATGCCATTCT-3'
		DrEF1a_R2 (#2083)	5'-CACGACCCACAGGTACAGTT-3'

Quantification of mouse gene expression was performed using the qPCR method of relative quantification in technical triplicates on 10 ng cDNA per reaction using the following primers:

MmAcrc	Primer efficiency: 99.8%	MmAcrc_F	5'-AAAGGCTAGCTGTGTCGTGA-3'
		MmAcrc_R	5'-TGTCAGAAGTCTCATCTCCACTG-3'
MmRplp0	Primer efficiency: 94.6%	MmRplp_F	5'-CTGCACTCTCGCTTTCTGGA-3'
		MmRplp_R	5'-TGATGATGGAGTGTGGCACC-3'

Zebrafish genes were normalized to the housekeeping gene (HKG) *elongation factor 1α (eef1a1l1*). Mouse *Acrc* expression was normalized to the housekeeping gene *Rplp0*. The

quantitative RT-PCRs were performed on a 7300 Real-Time PCR System (Applied Biosystems) using Power SYBR Green PCR Master Mix (#4367659, Applied Biosystems) according to manufacturer's instructions. After initial denaturation at 95˚C for 10 min, 40 amplification cycles were performed with denaturation at 95˚C/15 s, annealing and elongation at 60˚C/1 min, all together followed by melting curve analysis. Data analysis was performed using the 7500 Fast System SDS software (Applied Biosystems) and by applying the relative quantification method[46], which is based on the following formula yielding the Mean Normalized Expression (MNE):

$$MNE = E(HKG)^{Ct\ (HKG)} \ / \ E(gene)^{Ct\ (gene)},$$

E (HKG) – amplification efficiency of the housekeeping gene, Ct (HKG) – average Ct value of the HKG for a particular tissue, E (gene) – amplification efficiency of the gene of interest, Ct (gene) – average Ct value of the gene of interest for that particular tissue. Data is given as MNE*10^6 ± S.E.M.

Isolation and detection of DPCs by SDS-KCl method

Isolation of DPCs was performed using the SDS/KCl precipitation assay based on Zhitkovich and Costa (1992)[26] and adapted from Mórocz et al. (2017)[8]. This method was used for DPC isolation from zebrafish embryos treated with 5mM of the DPC-inducing agent formaldehyde (FA) for 1 hour at 28.5°C and from untreated embryos. The following samples were collected: WT and progeny of incrossed heterozygous *acrc*$^{rbi5/+}$ parents, i.e. 25% WT, 50% heterozygotes and 25% mutants. For isolation of DPCs using the KCl/SDS precipitation assay, 10 embryos per sample were pooled at 3 dpf and lysed in 400 µl lysis buffer (2% SDS; 20 mM Tris, pH 7.5) and then incubated for 15 minutes at room temperature. Similarly, pools of 100 untreated embryos were collected at 6 hpf and further processed for DPC quantifications; here, the following samples were collected: WT and *acrc*$^{rbi8/9}$ maternal mutants. Samples were then placed in liquid nitrogen and incubated overnight. The next day, samples were thawed in a thermoblock (55°C/15 min) and then sonicated. Proteins were then precipitated by adding 400 µl KCl buffer (200 mM KCl; 20 mM Tris, pH 7.5) followed by incubation on ice for 5 min. The precipitated proteins were pelleted by centrifugation at 21,000 g for 5 min (4°C), and the supernatant was kept for quantification of soluble DNA. The pellet was washed three times by adding 400 µl KCl buffer, followed by incubation at 55°C for 5 min, 5 min on ice, and centrifugation at 15,000 g at 4°C for 5 min. After washing, each pellet was resuspended in 400 µl KCl buffer containing proteinase K (0.2 mg/ml) and incubated at 55°C for 1h. After incubation, BSA (1.25 mg/ml) was added and samples were incubated on ice for 5 min. After centrifugation at 15,000 g at 4°C for 5 min, the supernatant contained the cross-linked DNA. From both the soluble and cross-linked DNA, 50 µl of the sample was taken for treatment with RNase A (0.2 mg/ml) for 30 min at 37°C. Soluble DNA and cross-linked DNA were quantified using the Quant-iT™ 1X dsDNA HS assay (ThermoFischer Scientific, MA, USA), and the amount of DPCs was calculated as the ratio of cross-linked DNA to total DNA (soluble + cross-linked).

Isolation and detection of DPCs by RADAR method

DPC isolation and detection from zebrafish embryos was performed using the RADAR (rapid approach to DNA adduct recovery) assay[27]. DPCs were isolated from 2 embryos as follows for each sample: (1) lysis of a pool of 25 embryos (at 2 dpf) or 50 embryos (at 6 hpf) with pre-warmed

lysis buffer (6 M GTC, 10 mM Tris-HCl (pH 6.8), 20 mM EDTA, 4% Triton X100, 1% N-lauroylsarcosine sodium, and 1% dithiothreitol) for 10 min at 55 °C with vigorous mixing; (2) addition of an equal volume of 98 % ethanol to precipitate DNA with crosslinked proteins; (3) centrifugation at 10000 rcf for 10 min at 4 °C; (4) washing the pellet four times with wash buffer (20 mM Tris (pH 7.4), 1mM EDTA, 50 mM NaCl, 50% EtOH) with the same centrifugation steps as in (3); (4) dissolving the pellet in 8 mM NaOH. A small aliquot of the DPC sample was treated with proteinase K (15 μg, Fisher Scientific, BP1700-100), and the remaining DNA was quantified using PicoGreen according to the manufacturer's instructions (Invitrogen, P7581). All DPC samples were normalized to that with the same amount of DNA and treated with DNAse (Millipore, E1014) for 1 h at 37 °C, followed by snap-freezing in liquid nitrogen and subsequent overnight lyophilization. They were then dissolved in SDS loading buffer (4 M urea, 62.5 mM Tris-HCl (pH 6.8), 1 mM EDTA, 2% SDS) and total DPCs were resolved on a SDS-PAGE gradient gel (5-18%) followed by silver staining, according to the manufacturer's protocol (Sigma Aldrich, PROTSIL1). For the detection of histone H3, a DPC amount of 150 ng DPC-DNA (for 2dpf embryo samples) or 50 ng DPC-DNA (for 6 hpf embryo samples) was subjected to western blotting and immunostained with the anti-H3 antibody (Cell Signaling, #9715, 1:3000). Briefly, DPCs were resolved on 5-18% SDS-PAGE gradient gels and transferred to a PVDF membranes (Roche, 03010040001). Membranes were blocked with 5% low-fat milk in TBST buffer (10mM TrisHCl (pH 7.5), 15mM NaCl, 0.02% Tween 20) for 2 hours at RT and then incubated with the primary antibody in 2.5% BSA in TBST overnight at +4°C, followed by an incubation with an HRP-labelled anti-rabbit secondary antibody (Sigma-Aldrich, #a0545, 1:100000) for 1 hour and washed three times for 15 minutes in TBST buffer. Detection was performed according to the manufacturer's instructions for the ECL blotting substrate (Biorad, #1705061) and visualized using the ChemiDoc™ XRS+ System (Bio-Rad, #1708299). DNA detection was performed by applying 2 ng of the sample used for PicoGreen detection to a nylon membrane and detecting with the anti-dsDNA antibody (Abcam #ab27156, 1:9000).

Statistical Analysis

Data show are means with S.E.M. Data was statistically analyzed using the Prism software (v.8.0.1, GraphPad) as described below. Changes were statistically significant with $P < 0.05$.

1) Figure 3A-B: quantification of relative gene expression levels for *acrc* and *sprtn* in adult zebrafish tissues normalized to *eef1a1l1* housekeeping gene expression: an unpaired Student's t-test was performed for each tissue to determine whether gene expression is significantly dependent on gender. Differences were not significant, except for *acrc* levels in kidney (*: p-value = 0.0451) and in gonads (**: p-value = 0.0013).
2) Figure 3C: quantification of relative gene expression levels for *Acrc* in adult mouse tissues normalized to *Rplp0* housekeeping gene expression: an unpaired Student's t-test was performed for each tissue to determine whether gene expression is significantly dependent on gender. Differences were not significant, except in gonads (*: p-value = 0.0114).
3) Figure 3D: quantification of gene expression levels for *acrc* and *sprtn* during zebrafish embryonic development normalized to *eef1a1l1* housekeeping gene expression. Each gene was analyzed separately and One-way ANOVA analyses were followed by Sidak's

multiple comparisons tests. Gene expression levels were compared separately within the first 6 hours post fertilization (maternal mRNA contribution) and between 6 hpf – 72 hpf (zygotic gene expression). For *acrc*, expression levels significantly dropped between 1 hpf and 6 hpf (*: p-value = 0.0297), but no other changes were significant.

4) Supplemental Figure S7C, Supplemental Table 3: quantifications of rescue levels: percentage of live embryos after 1 dpf: non-injected WT (n= 15 experiments, 698 embryos; 96.27 ± 1.6% alive), WT injected with WT DrAcrc (#553) (n= 7 experiments, 278 embryos; 94.11 ± 2.44% alive), uninjected *acrc* maternal mutant embryos (n=10 experiments, 490 embryos; 1.36 ± 0.76% alive) and rescued *acrc* maternal mutant embryos with WT DrAcrc (#553) (n=5 experiments, 495 embryos; 93.89 ± 1.16% alive). A 2-way ANOVA followed by Tukey's test was performed. ****: p-value < 0.0001.
5) Figure 7A: quantification of DPC levels (% of crosslinked DNA / free DNA) as measured by the SDS-KCl method. In comparison to WT embryos, *acrc*$^{rbi8/rbi9}$ mutant embryos display a significant increase in total DPC levels at 6 hpf. An unpaired Student's t-test was performed for 3 biological replicates, pools of 100 embryos each (***: p-value = 0.0254).
6) Figure 7B: quantification of total DPCs based on silver stainings shown here and in Supplemental Figure S9A. In comparison to WT embryos, *acrc*$^{rbi5/rbi5}$ mutant embryos display a significant increase in total DPC levels at 6 hpf. An unpaired Student's t-test was performed for 4 biological replicates, pools of 50 embryos each (****: p-value < 0.0001). The same stainings were subdivided according to molecular weight (low: < 40 kDa, middle: 41-150 kDa, high: > 151 kDa) and quantified separately. An unpaired Student's t-test was performed for 3 (HMW) and 4 biological replicates (MMW and LMW) (****: p-value < 0.0001).
7) Figure 7C: quantification of H3-DPC levels based on western blots shown here and in Supplemental Figure S9B. In comparison to WT embryos, *acrc*$^{rbi5/rbi5}$ mutant embryos display a significant increase in H3-DPC levels at 6 hpf. An unpaired Student's t-test was performed for 3 biological replicates, pools of 50 embryos each (****: p-value < 0.0001).
8) Supplemental Figure S10B: quantification of total DPCs based on silver stainings shown in Supplemental Figure S10A. 2 dpf WT and *acrc*$^{rbi5/+}$ heterozygous embryos were treated with 10mM FA. A two-way ANOVA analysis was performed, followed by Tukey's multiple comparisons test, which revealed that the FA treatment significantly changed the total DPC levels in both WT and heterozygotes. 2 biological replicates, pools of 25 embryos each (**: p-value = 0.0022).
9) Supplemental Figure S11A: quantification of H3-DPC levels based on western blots shown here. 2 dpf WT and *acrc*$^{rbi5/+}$ heterozygous embryos were treated with 10mM FA. A two-way ANOVA analysis was performed, followed by Tukey's multiple comparisons test, which revealed that the FA treatment significantly changed the total DPC levels in both WT and heterozygotes. 2 biological replicates, pools of 25 embryos each (*: p-value = 0.0277).
10) Supplemental Figure S11B: quantification of DPC levels (% of crosslinked DNA / free DNA) as measured by the SDS-KCl method. In comparison to WT embryos, the progeny of *acrc*$^{rbi5/+}$heterozygous embryos display a significant increase in total DPC levels at 3 dpf upon FA treatment. Two-way ANOVA analysis followed by Tukey's multiple comparisons tests were performed for 3 biological replicates, pools of 10 embryos each. There is a

significant difference between FA-treated WT and FA-treated Acrc-deficient embryos: *: p-value = 0.0134; there is also a significant difference between untreatred and FA-treated Acrc-deficient embryos: *: p-value = 0.0198.

Supplemental information titles and legends

Supplemental Figure S1. Extended phylogenetic tree of ACRC/GCNA orthologs. Full-length protein sequences were aligned using MAFFT and the phylogenetic tree was constructed in PhyML. Blue: non-rodent mammals, dark blue: rodents and bats with a SprT-like domain, grey: rodents without SprT-like domain, green: birds, red: reptiles, yellow: amphibians, orange: fish, colorless: invertebrates.

Supplemental Figure S2. Extended phylogenetic tree of ACRC/GCNA orthologs. SprtT-like domains protein sequences were aligned using MAFFT and the phylogenetic tree was constructed in PhyML. Blue: non-rodent mammals, dark blue: rodents with a SprT-like domain, green: birds, red: reptiles, yellow: amphibians, orange: fish, colorless: invertebrates.

Supplemental Figure S3. Extended phylogenetic tree of ACRC/GCNA orthologs. N domain/non-structured N half protein sequences were aligned using MAFFT and the phylogenetic tree was constructed in PhyML. Blue: non-rodent mammals, dark blue: rodents and bats with a SprT-like domain, grey: rodents without SprT-like domain, green: birds, red: reptiles, yellow: amphibians, orange: fish, colorless: invertebrates.

Supplemental Figure S4. Conserved synteny analysis of zebrafish, mouse and human ACRC/GCNA genes. Numbers next to the gene names represent megabase pair (Mbp) of gene location on the chromosome. Chromosome segments are represented with blue (continuous segments). Orthologs are connected with lines. Grey background highlights regions with conserved gene order between mouse and human.

Supplemental Figure S5. Disorder disposition plot for human, zebrafish and mouse ACRC predicted using PONDR-FIT workspace. Values above 0.5. indicate disordered regions.

Supplemental Figure S6. Creation of two *acrc* mutant zebrafish strains. Scheme of the deleted domains in *acrc* mutant alleles *rbi5* and *rbi8* & *rbi9*. *rbi5* allele: the deletion of 12 basepairs leads to a 4 amino-acids deletion (DEMCH, aa 451-454) in the enzymatic core of the SprT-like domain of Acrc; *rbi8* allele: the insertion of 1 basepair leads to a premature stop codon at aa 477; *rbi9* allele: the indel of 11 basepairs leads to a premature stop codon at aa 472. Both *rbi8* and *rbi9* alleles result in a truncation of the C-terminus of Acrc, including half of the Sprtn domain. All 3 alleles were created using CrispR/Cas9 technology.

Supplemental Figure S7. WT Acrc mRNA injections fully rescue the *acrc* Δ-C-terminal maternal mutant phenotype. A – scheme of the injected rescue constructs: #553: DrAcrc-WT, #581: DrAcrc-E451A, #582: DrAcrc-DCterm, #583: DrAcrc-DSprtn, #584: DrAcrc-IDR, #585: DrAcrc-DR/K/P. B – phenotype characterization of rescued embryos with representative pictures. WT and *acrc* D-C-terminal maternal mutant embryos (*acrc*$^{rbi8\ and/or\ rbi9}$) were injected with 1nl of 250ng/µl RNA

derived from the rescue constructs described above. Phenotypes were scored at 1 dpf and divided into 5 categories: #1: dead, #2: necrotic, #3: very abnormal, #4: abnormal, #5: WT-like. Embryos in categories #3, 4 and 5 were considered alive. C – survival of non-injected WT (96.27 ± 1.6% alive), WT injected with WT DrAcrc (#553) (94.11 ± 2.44% alive), uninjected *acrc* maternal mutant embryos (1.36 ± 0.76% alive) and rescued *acrc* maternal mutant embryos with WT DrAcrc (#553) (93.89 ± 1.16% alive). For detailed results, see Supplemental Table 3. Data shown are means.

Supplemental Figure S8. mRNAs expressed from the rescue constructs are enriched in WT. A - RT-qPCR results showing the upregulation of zebrafish *acrc* in WT embryos injected with the following DrAcrc rescue constructs at 2 dpf relative to uninjected WT: DrAcrc (WT) (#553), DrAcrcE451A (#581), DrAcrcDCterm (#582), DrAcrcDSprtn (#583). DrSprtn expression was normalized to Dr18S. The cDNAs were obtained from 1 pool of 20 embryos for each sample. B - RT-qPCR results showing the upregulation of zebrafish *sprtn* in WT embryos injected with the DrSprtn rescue construct (#603) at 1 dpf relative to uninjected WT. DrSprtn expression was normalized to Dr18S. The cDNAs were obtained from 1 pool of 5 embryos for each sample. C – PCR products of *Atp50* amplification (as housekeeping gene, 93 bp) and of mouse *Acrc* amplification (107 bp) on cDNA derived from 2 dpf non-injected WT and WT injected with RNA from rescue construct #608 encoding full-length mouse Acrc cds (1 pool of 20 embryos each). L = DNA ladder.

Supplemental Figure S9. DPC measurements in 6 hpf zebrafish *acrc* mutant embryos by RADAR. A – Total DPCs isolated from WT and $acrc^{rbi5/rbi5}$ homozygous maternal mutants were separated on an SDS acrylamide gel and stained with silver. Dot blots beneath show equal dsDNA loading; the equivalent of 50 ng of DNA was loaded per well. Shown are 4 biological replicates whose quantification is shown in Figure 7B. B – Histone H3-DPC detection by western blot, with dot blot for dsDNA. Shown are 5 biological replicates whose quantification is shown in Figure 7C. L = ladder.

Supplemental Figure S10. DPC measurements in zebrafish embryos with reduced Acrc levels. RADAR assays followed by SDS acrylamide gel separation and silver staining of DPCs from 2 dpf WT and *rbi5* heterozygous embryos treated or not with 10 mM FA for 30 minutes. Shown are biological duplicates, with low exposure (top) and high exposure (bottom). Quantifications of the staining intensities normalized to WT are shown in B. Dot blot for dsDNA shows equal loading; total DPCs were normalized to DNA and an equivalent of 150 ng of DNA was loaded per well. A two-way ANOVA analysis was performed, followed by Tukey's multiple comparisons test; **: p-value = 0.0022. L = ladder. Data shown are means with S.E.M.

Supplemental Figure S11. DPC measurements in zebrafish embryos with reduced Acrc levels. A – RADAR assays followed by histone H3-DPC detection by western blot, with dot blot for dsDNA as a loading control (the equivalent of 150 ng of DNA was loaded per well). Shown are 2 biological duplicates and the quantification of H3 staining intensities normalized to WT. RADAR performed on 2 dpf WT and *rbi5* heterozygous embryos treated or not with 10 mM FA for 30 minutes. A two-way ANOVA analysis was performed, followed by Tukey's multiple comparisons test; *: p-value = 0.0277. B – Total DPC levels (percentage of DNA-protein crosslinks vs. free DNA) as quantified using the KCl/SDS method. DPC levels quantified in 3dpf embryos after exposure to 5

mM formaldehyde (FA) for 1 hour. Acrc samples consist in the progeny of incrossed heterozygous *acrc*$^{rbi5/+}$ parents: 25% WT, 50% heterozygotes and 25% mutants; all embryos are viable due to maternal Acrc deposition in the eggs. Two-way ANOVA analysis followed by Tukey's multiple comparisons tests were performed for 3 biological replicates, pools of 10 embryos each; *: p-value < 0.05. L = ladder. Data shown are means with S.E.M; ns = not significant.

Supplemental Table 1. Protein sequences used for building the phylogenetic tree of full length ACRC/GCNA orthologs. Accession numbers in NCBI database, species abbreviations and group designations.

Supplemental Table 2. Rescue experiments with the DrAcrc rescue constructs #553, 581-585 in the *acrc* D-EMCH maternal mutant fish. Raw data: numbers of embryos in each assessment category at 1 dpf. Rbi5 mutant line: percentage of embryos in each assessment category for each experiment.

Supplemental Table 3. Rescue experiments with the DrAcrc rescue constructs #553, 581-585 in the *acrc* D-C-terminal maternal mutant fish. Raw data: numbers of embryos in each assessment category at 1 dpf. Rbi8-9 mutant line: percentage of embryos in each assessment category for each experiment.

Supplemental Table 4. Rescue experiments with the DrSprtn and the MmAcrc rescue constructs in the *acrc* D-EMCH maternal mutant fish. Raw data: numbers of embryos in each assessment category at 1 dpf. Rbi5 mutant line: percentage of embryos in each assessment category for each experiment.

1. Ruggiano, A., and Ramadan, K. (2021). DNA-protein crosslink proteases in genome stability. Communications Biology *4*, 11. 10.1038/s42003-020-01539-3.

2. Borgermann, N., Ackermann, L., Schwertman, P., Hendriks, I.A., Thijssen, K., Liu, J.C., Lans, H., Nielsen, M.L., and Mailand, N. (2019). SUMOylation promotes protective responses to DNA-protein crosslinks. The EMBO journal *38*, e101496. 10.15252/embj.2019101496.

3. Larsen, N.B., Gao, A.O., Sparks, J.L., Gallina, I., Wu, R.A., Mann, M., Räschle, M., Walter, J.C., and Duxin, J.P. (2019). Replication-Coupled DNA-Protein Crosslink Repair by SPRTN and the Proteasome in Xenopus Egg Extracts. Molecular Cell *73*, 574-588.e7. 10.1016/j.molcel.2018.11.024.

4. Stingele, J., Schwarz, M.S., Bloemeke, N., Wolf, P.G., and Jentsch, S. (2014). A DNA-dependent protease involved in DNA-protein crosslink repair. Cell *158*, 327–338. 10.1016/j.cell.2014.04.053.

5. Stingele, J., Bellelli, R., Alte, F., Hewitt, G., Sarek, G., Maslen, S.L., Tsutakawa, S.E., Borg, A., Kjær, S., Tainer, J.A., et al. (2016). Mechanism and Regulation of DNA-Protein Crosslink Repair by the DNA-Dependent Metalloprotease SPRTN. Mol Cell *64*, 688–703. 10.1016/j.molcel.2016.09.031.

6. Vaz, B., Popovic, M., Newman, J.A., Fielden, J., Aitkenhead, H., Halder, S., Singh, A.N., Vendrell, I., Fischer, R., Torrecilla, I., et al. (2016). Metalloprotease SPRTN/DVC1 Orchestrates Replication-Coupled DNA-Protein Crosslink Repair. Molecular Cell *64*, 704–719. 10.1016/j.molcel.2016.09.032.

7. Lopez-Mosqueda, J., Maddi, K., Prgomet, S., Kalayil, S., Marinovic-Terzic, I., Terzic, J., and Dikic, I. (2016). SPRTN is a mammalian DNA-binding metalloprotease that resolves DNA-protein crosslinks. Elife *5*, e21491. 10.7554/eLife.21491.

8. Mórocz, M., Zsigmond, E., Tóth, R., Enyedi, M.Z., Pintér, L., and Haracska, L. (2017). DNA-dependent protease activity of human Spartan facilitates replication of DNA–protein crosslink-containing DNA. Nucleic Acids Research *45*, 3172–3188. 10.1093/nar/gkw1315.

9. Maskey, R.S., Flatten, K.S., Sieben, C.J., Peterson, K.L., Baker, D.J., Nam, H.-J., Kim, M.S., Smyrk, T.C., Kojima, Y., Machida, Y., et al. (2017). Spartan deficiency causes accumulation of Topoisomerase 1 cleavage complexes and tumorigenesis. Nucleic Acids Res *45*, 4564–4576. 10.1093/nar/gkx107.

10. Dokshin, G.A., Davis, G.M., Sawle, A.D., Eldridge, M.D., Nicholls, P.K., Gourley, T.E., Romer, K.A., Molesworth, L.W., Tatnell, H.R., Ozturk, A.R., et al. (2020). GCNA Interacts with Spartan and Topoisomerase II to Regulate Genome Stability. Developmental Cell *52*, 53-68.e6. 10.1016/j.devcel.2019.11.006.

11. Bhargava, V., Goldstein, C.D., Russell, L., Xu, L., Ahmed, M., Li, W., Casey, A., Servage, K., Kollipara, R., Picciarelli, Z., et al. (2020). GCNA Preserves Genome Integrity and Fertility Across Species. Developmental Cell *52*, 38-52.e10. 10.1016/j.devcel.2019.11.007.

12. Kojima, Y., Machida, Y., Palani, S., Caulfield, T.R., Radisky, E.S., Kaufmann, S.H., and Machida, Y.J. (2020). FAM111A protects replication forks from protein obstacles via its trypsin-like domain. Nat Commun *11*, 1318. 10.1038/s41467-020-15170-7.

13. Hoffmann, S., Pentakota, S., Mund, A., Haahr, P., Coscia, F., Gallo, M., Mann, M., Taylor, N.M., and Mailand, N. (2020). FAM111 protease activity undermines cellular fitness and is amplified by gain-of-function mutations in human disease. EMBO Rep *21*, e50662. 10.15252/embr.202050662.

14. Nowicka, U., Zhang, D., Walker, O., Krutauz, D., Castañeda, C.A., Chaturvedi, A., Chen, T.Y., Reis, N., Glickman, M.H., and Fushman, D. (2015). DNA-damage-inducible 1 protein (Ddi1) contains an uncharacteristic ubiquitin-like domain that binds ubiquitin. Structure *23*, 542–557. 10.1016/j.str.2015.01.010.

15. Kottemann, M.C., Conti, B.A., Lach, F.P., and Smogorzewska, A. (2018). Removal of RTF2 from Stalled Replisomes Promotes Maintenance of Genome Integrity. Mol Cell *69*, 24-35.e5. 10.1016/j.molcel.2017.11.035.

16. Serbyn, N., Noireterre, A., Bagdiul, I., Plank, M., Michel, A.H., Loewith, R., Kornmann, B., and Stutz, F. (2020). The Aspartic Protease Ddi1 Contributes to DNA-Protein Crosslink Repair in Yeast. Mol Cell *77*, 1066-1079.e9. 10.1016/j.molcel.2019.12.007.

17. Svoboda, M., Konvalinka, J., Trempe, J.-F., and Grantz Saskova, K. (2019). The yeast proteases Ddi1 and Wss1 are both involved in the DNA replication stress response. DNA Repair (Amst) *80*, 45–51. 10.1016/j.dnarep.2019.06.008.

18. Yip, M.C.J., Bodnar, N.O., and Rapoport, T.A. (2020). Ddi1 is a ubiquitin-dependent protease. Proc Natl Acad Sci U S A *117*, 7776–7781. 10.1073/pnas.1902298117.

19. Dirac-Svejstrup, A.B., Walker, J., Faull, P., Encheva, V., Akimov, V., Puglia, M., Perkins, D., Kümper, S., Hunjan, S.S., Blagoev, B., et al. (2020). DDI2 Is a Ubiquitin-Directed Endoprotease Responsible for Cleavage of Transcription Factor NRF1. Mol Cell *79*, 332-341.e7. 10.1016/j.molcel.2020.05.035.

20. Carmell, M.A., Dokshin, G.A., Skaletsky, H., Hu, Y.-C., van Wolfswinkel, J.C., Igarashi, K.J., Bellott, D.W., Nefedov, M., Reddien, P.W., Enders, G.C., et al. (2016). A widely employed germ cell marker is an ancient disordered protein with reproductive functions in diverse eukaryotes. eLife *5*, e19993. 10.7554/eLife.19993.

21. Lessel, D., Vaz, B., Halder, S., Lockhart, P.J., Marinovic-Terzic, I., Lopez-Mosqueda, J., Philipp, M., Sim, J.C.H., Smith, K.R., Oehler, J., et al. (2014). Mutations in SPRTN cause early onset hepatocellular carcinoma, genomic instability and progeroid features. Nature Genetics *46*, 1239–1244. 10.1038/ng.3103.

22. Hardy, J.J., Wyrwoll, M.J., Mcfadden, W., Malcher, A., Rotte, N., Pollock, N.C., Munyoki, S., Veroli, M.V., Houston, B.J., Xavier, M.J., et al. (2021). Variants in GCNA, X-linked germ-cell genome integrity gene, identified in men with primary spermatogenic failure. Human Genetics *140*, 1169–1182. 10.1007/s00439-021-02287-y.

23. Howe, K., Clark, M.D., Torroja, C.F., Torrance, J., Berthelot, C., Muffato, M., Collins, J.E., Humphray, S., McLaren, K., Matthews, L., et al. (2013). The zebrafish reference genome sequence and its relationship to the human genome. Nature *496*, 498–503. 10.1038/nature12111.

24. Tadros, W., and Lipshitz, H.D. (2009). The maternal-to-zygotic transition: a play in two acts. Development *136*, 3033–3042. 10.1242/dev.033183.

25. Carmell, M.A., Dokshin, G.A., Skaletsky, H., Hu, Y.C., van Wolfswinkel, J.C., Igarashi, K.J., Bellott, D.W., Nefedov, M., Reddien, P.W., Enders, G.C., et al. (2016). A widely employed germ cell marker is an ancient disordered protein with reproductive functions in diverse eukaryotes. eLife *5*, 1–25. 10.7554/eLife.19993.

26. Zhitkovich, A., and Costa, M. (1992). A simple, sensitive assay to detect DNA-protein crosslinks in intact cells and in vivo. Carcinogenesis *13*, 1485–1489. 10.1093/carcin/13.8.1485.

27. Kiianitsa, K., and Maizels, N. (2013). A rapid and sensitive assay for DNA–protein covalent complexes in living cells. Nucleic Acids Research *41*, e104. 10.1093/nar/gkt171.

28. Uhlén, M., Fagerberg, L., Hallström, B.M., Lindskog, C., Oksvold, P., Mardinoglu, A., Sivertsson, Å., Kampf, C., Sjöstedt, E., Asplund, A., et al. (2015). Tissue-based map of the human proteome. Science *347*, 1260419. 10.1126/science.1260419.

29. Ribeiro, J., and Crossan, G.P. (2022). GCNA is a histone binding protein required for spermatogonial stem cell maintenance. 10.1101/2022.02.21.481287.

30. Pachva, M.C., Kisselev, A.F., Matkarimov, B.T., Saparbaev, M., and Groisman, R. (2020). DNA-Histone Cross-Links: Formation and Repair. Frontiers in Cell and Developmental Biology *8*.

31. Akdogan-Ozdilek, B., Duval, K.L., and Goll, M.G. (2020). Chromatin dynamics at the maternal to zygotic transition: recent advances from the zebrafish model. F1000Research *9*, F1000 Faculty Rev-299. 10.12688/f1000research.21809.1.

32. Edgar, R.C. (2004). MUSCLE: a multiple sequence alignment method with reduced time and space complexity. BMC Bioinformatics *5*, 113. 10.1186/1471-2105-5-113.

33. Guindon, S., and Gascuel, O. (2003). A simple, fast, and accurate algorithm to estimate large phylogenies by maximum likelihood. Syst Biol *52*, 696–704. 10.1080/10635150390235520.

34. Louis, A., Muffato, M., and Crollius, H.R. (2013). Genomicus: Five genome browsers for comparative genomics in eukaryota. Nucleic Acids Research *41*, 700–705. 10.1093/nar/gks1156.

35. Brendel, V., Bucher, P., Nourbakhsh, I.R., Blaisdell, B.E., and Karlin, S. (1992). Methods and algorithms for statistical analysis of protein sequences. Proceedings of the National Academy of Sciences of the United States of America *89*, 2002–2006. 10.1073/pnas.89.6.2002.

36. Paysan-Lafosse, T., Blum, M., Chuguransky, S., Grego, T., Pinto, B.L., Salazar, G.A., Bileschi, M.L., Bork, P., Bridge, A., Colwell, L., et al. (2023). InterPro in 2022. Nucleic Acids Research *51*, D418–D427. 10.1093/nar/gkac993.

37. Sigrist, C.J.A., de Castro, E., Cerutti, L., Cuche, B.A., Hulo, N., Bridge, A., Bougueleret, L., and Xenarios, I. (2013). New and continuing developments at PROSITE. Nucleic Acids Research *41*, D344–D347. 10.1093/nar/gks1067.

38. Liu, W., Xie, Y., Ma, J., Luo, X., Nie, P., Zuo, Z., Lahrmann, U., Zhao, Q., Zheng, Y., Zhao, Y., et al. (2015). IBS: an illustrator for the presentation and visualization of biological sequences. Bioinformatics *31*, 3359–3361. 10.1093/bioinformatics/btv362.

39. Jumper, J., Evans, R., Pritzel, A., Green, T., Figurnov, M., Ronneberger, O., Tunyasuvunakool, K., Bates, R., Žídek, A., Potapenko, A., et al. (2021). Highly accurate protein structure prediction with AlphaFold. Nature *596*, 583–589. 10.1038/s41586-021-03819-2.

40. Varadi, M., Anyango, S., Deshpande, M., Nair, S., Natassia, C., Yordanova, G., Yuan, D., Stroe, O., Wood, G., Laydon, A., et al. (2022). AlphaFold Protein Structure Database: massively expanding the structural coverage of protein-sequence space with high-accuracy models. Nucleic Acids Research *50*, D439–D444. 10.1093/nar/gkab1061.

41. Pettersen, E.F., Goddard, T.D., Huang, C.C., Couch, G.S., Greenblatt, D.M., Meng, E.C., and Ferrin, T.E. (2004). UCSF Chimera–a visualization system for exploratory research and analysis. Journal of Computational Chemistry *25*, 1605–1612. 10.1002/jcc.20084.

42. Xue, B., Dunbrack, R.L., Williams, R.W., Dunker, A.K., and Uversky, V.N. (2010). PONDR-FIT: a meta-predictor of intrinsically disordered amino acids. Biochimica Et Biophysica Acta *1804*, 996–1010. 10.1016/j.bbapap.2010.01.011.

43. Kimmel, C.B., Ballard, W.W., Kimmel, S.R., Ullmann, B., and Schilling, T.F. (1995). Stages of embryonic development of the zebrafish. Developmental Dynamics: An Official Publication of the American Association of Anatomists *203*, 253–310. 10.1002/aja.1002030302.

44. Modzelewski, A.J., Chen, S., Willis, B.J., Lloyd, K.C.K., Wood, J.A., and He, L. (2018). Efficient mouse genome engineering by CRISPR-EZ technology. Nature Protocols *13*, 1253–1274. 10.1038/nprot.2018.012.

45. Rohr, S., Bit-Avragim, N., and Abdelilah-Seyfried, S. (2006). Heart and soul/PRKCi and nagie oko/Mpp5 regulate myocardial coherence and remodeling during cardiac morphogenesis. Development (Cambridge, England) *133*, 107–115. 10.1242/dev.02182.

46. Muller, P.Y., Janovjak, H., Miserez, A.R., and Dobbie, Z. (2002). Processing of gene expression data generated by quantitative real-time RT-PCR. BioTechniques *32*, 1372–1374, 1376, 1378–1379.

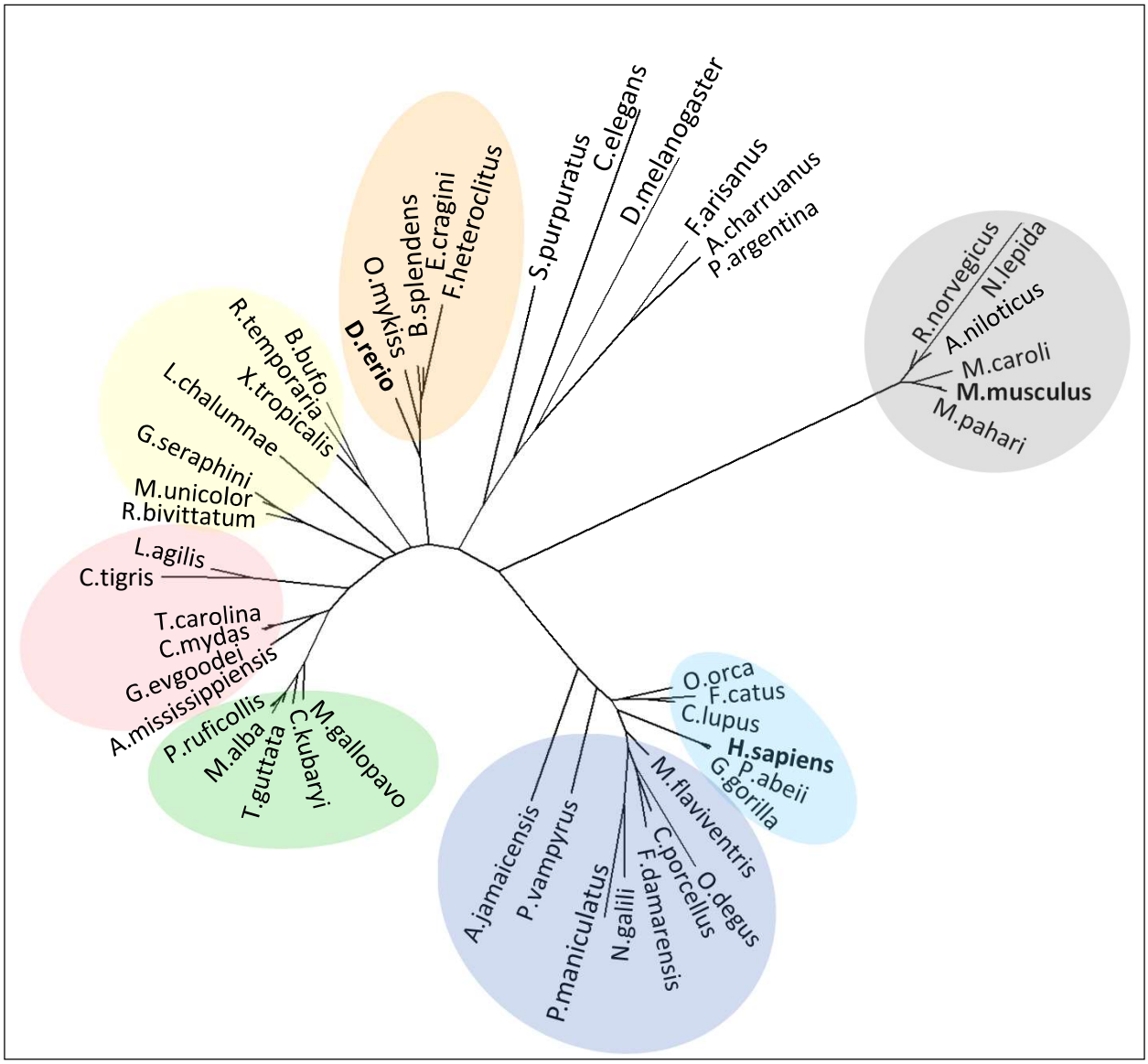

Figure 1. Phylogenetic analysis of ACRC/GCNA orthologs. Full-length (LG 4) protein sequences were aligned using MAFFT and the phylogenetic tree was constructed in PhyML. Blue: non-rodents mammals, dark blue: rodents and bats with a SprT-like domain, grey: rodents without SprT-like domain, green: birds, red: reptiles, yellow: amphibians, orange: fish, colorless: invertebrates.

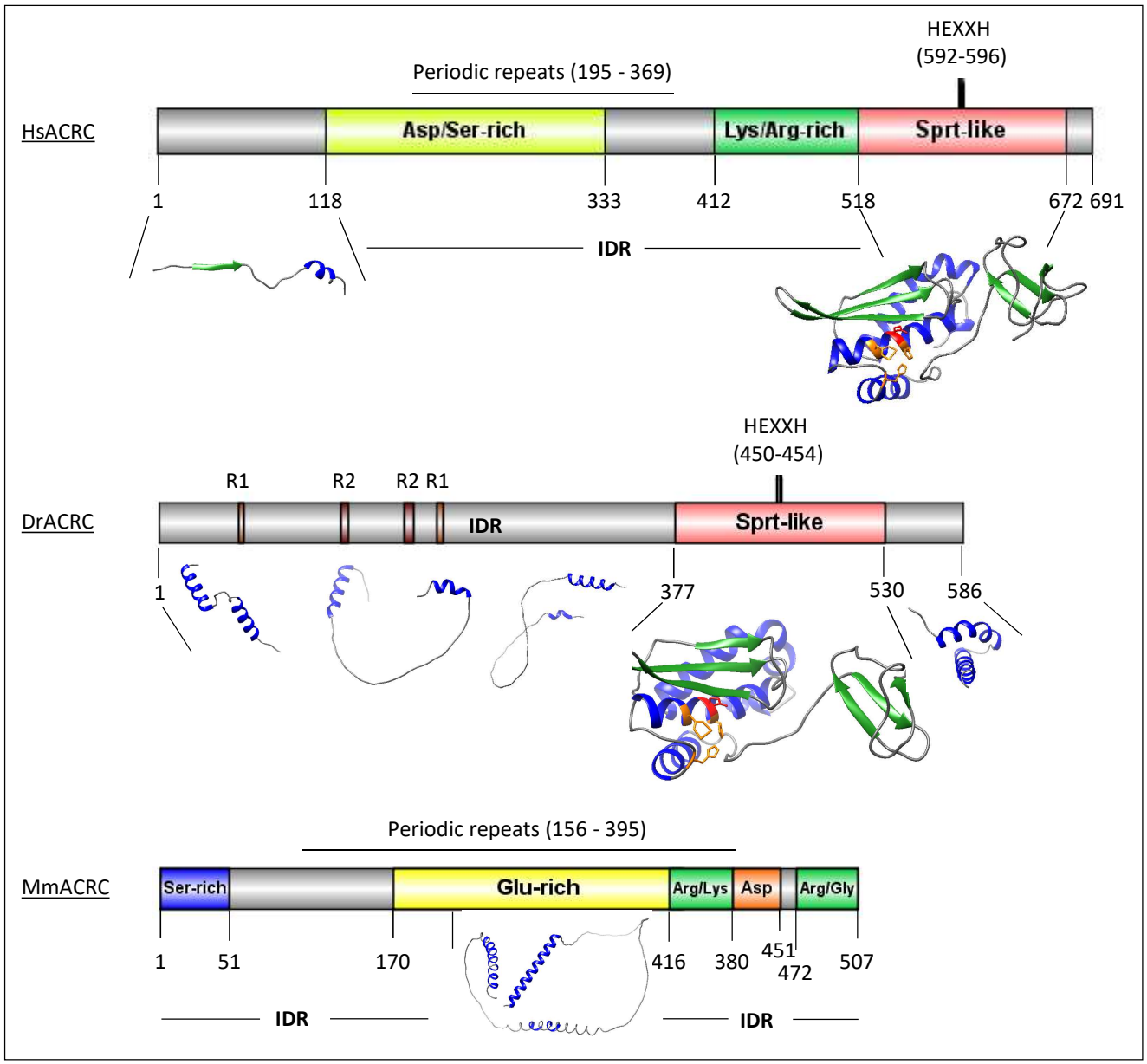

Figure 2. Comparison of human, zebrafish and mouse ACRC/GCNA protein domains and motifs and structural model of human ACRC. Domains and motifs were identified using SAPS and Motif Scan workspace. Models were build using Alphafold and analyzed with Chimera. HEXXH, protease core; IDR, Intrinsically Disordered Region; R, repeats. The metalloprotease core of ACRC includes the active glutamate shown in red and Zn^{2+} binding histidines shown in orange.

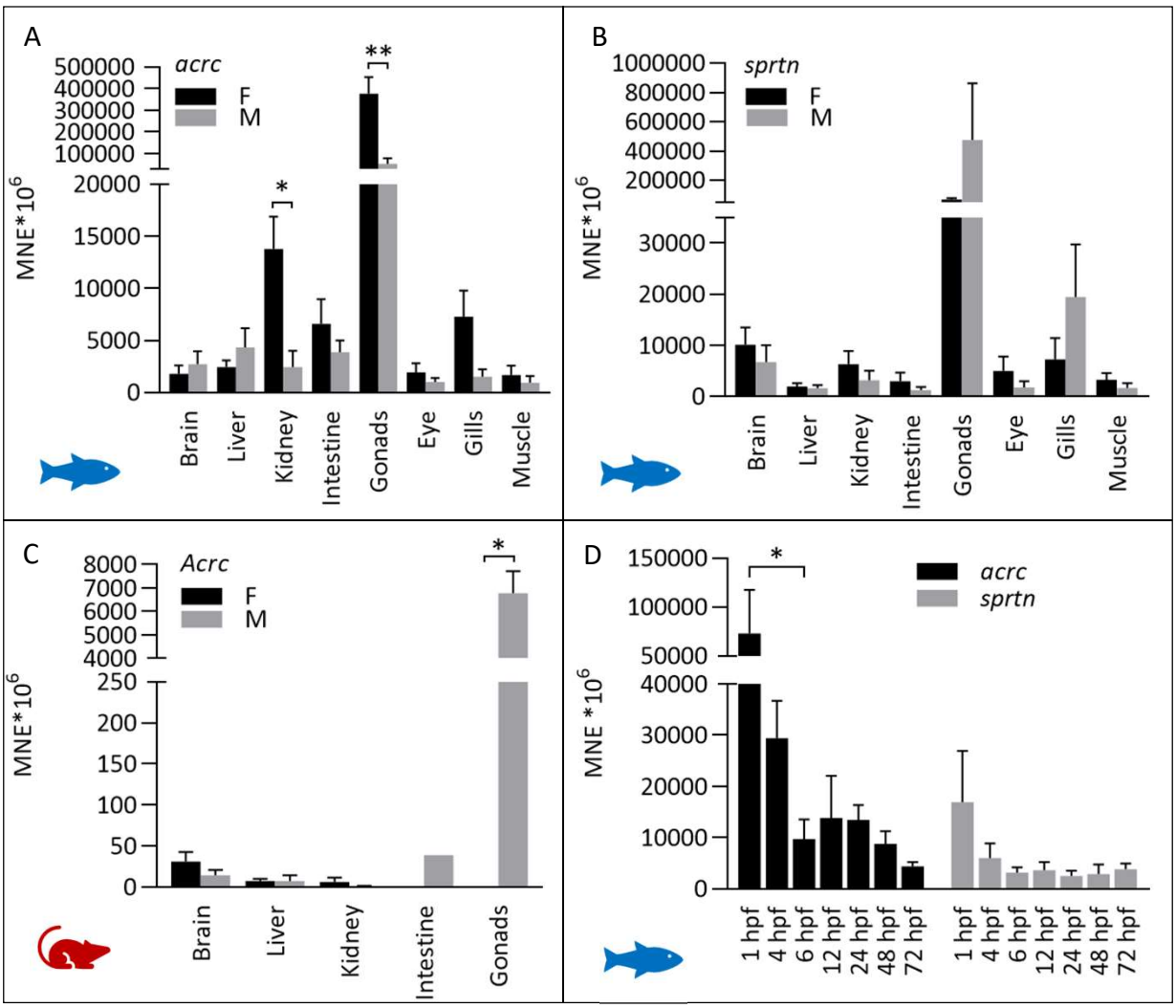

Figure 3. Expression patterns of *acrc* in comparison with *sprtn* quantified by qRT-PCR. A, B - Expression levels of *acrc* (A) and *sprtn* (B) in tissues of adult zebrafish. The only significant change in gene expression for *acrc* between male and female was in kidneys and gonads. C - Expression levels of *Acrc* in tissues of adult mice. The only significant change in gene expression for *Acrc* between male and female was in gonads. D - Comparison of *acrc* and *sprtn* expression levels in zebrafish embryos at 1, 4, 6, 12, 24, 48 and 72 hpf. The only significant change in gene expression was between 1 and 6 hpf for *acrc.* Data represent MNE (Mean Normalized Expression) ± S.E.M. normalized to the housekeeping genes *elongation factor 1α (eef1a1l1*) for zebrafish and *Rplp0* for mouse. F = female; M = male.

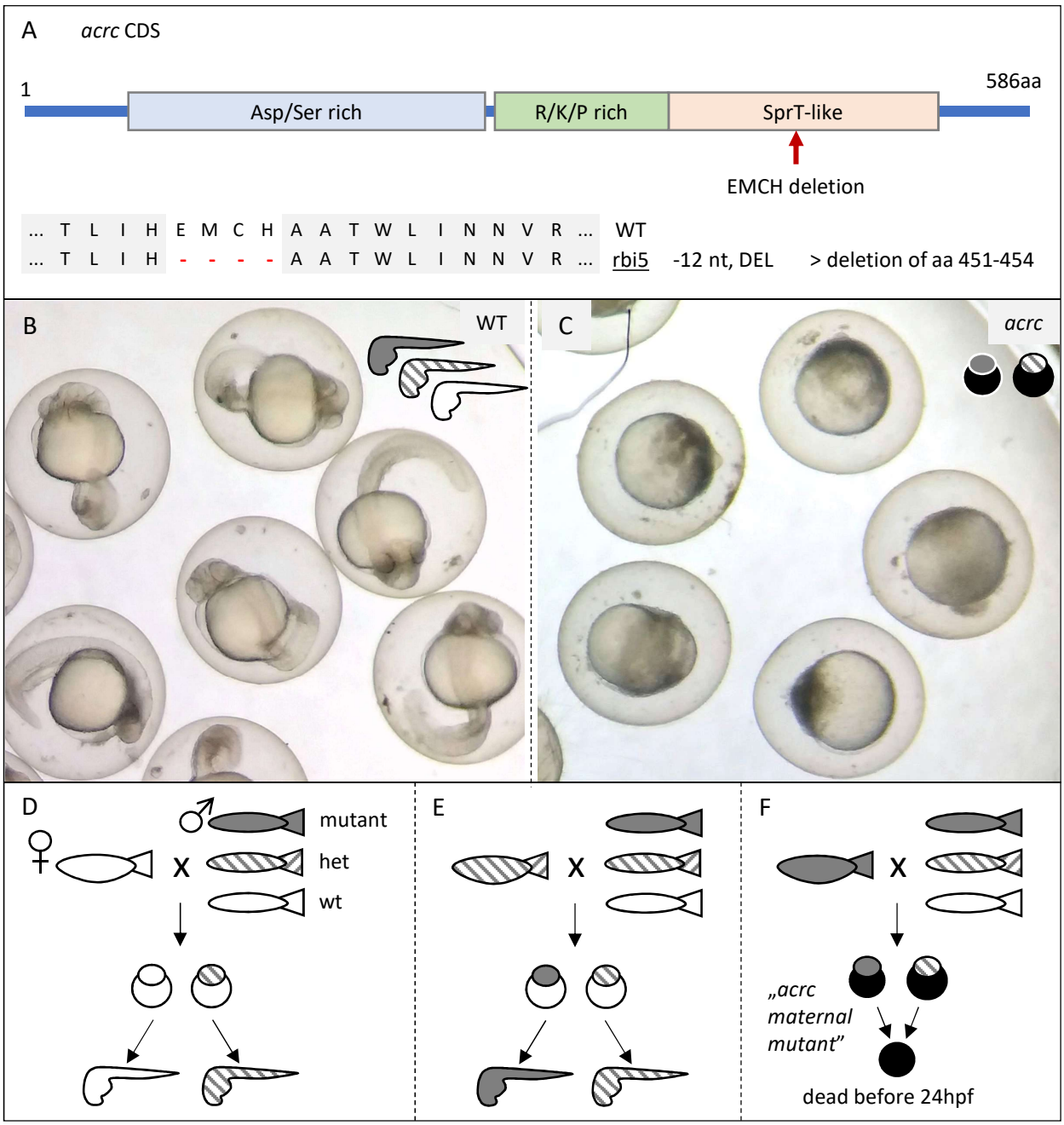

Figure 4. Creation of two *acrc* mutant zebrafish strains. A - Scheme of the Acrc protein and the position of the 4 amino-acids deletion (ΔEMCH, aa 451-454) in the enzymatic core of the SprT-like domain in the *rbi5* allele, which was created using CrispR/Cas9 technology. B, C – representative pictures of 1dpf embryos: WT (B) and *acrc* maternal mutants (C). D-F: schemes representing the genotype-phenotype correlations upon loss of one or both *acrc* wt alleles. D – crossing a wt female with any male (wt - white, heterozygote - stripes or mutant - grey) always leads to viable fish since heterozygous embryos are viable; E - crossing a heterozygous female with any male (wt, heterozygote or mutant) always leads to viable fish: Acrc is normally deposited in the egg and therefore even mutant embryos are viable; F - crossing an *acrc* mutant female with any male (wt, heterozygote or mutant) always results in embryos with an early lethal phenotype (black yolk), henceforth called „*acrc* phenotype", due to lack of Acrc deposition in the egg, irrespective of the genotype of the embryo itself (mutant or heterozygote); these embryos are henceforth called „maternal *acrc* mutants".

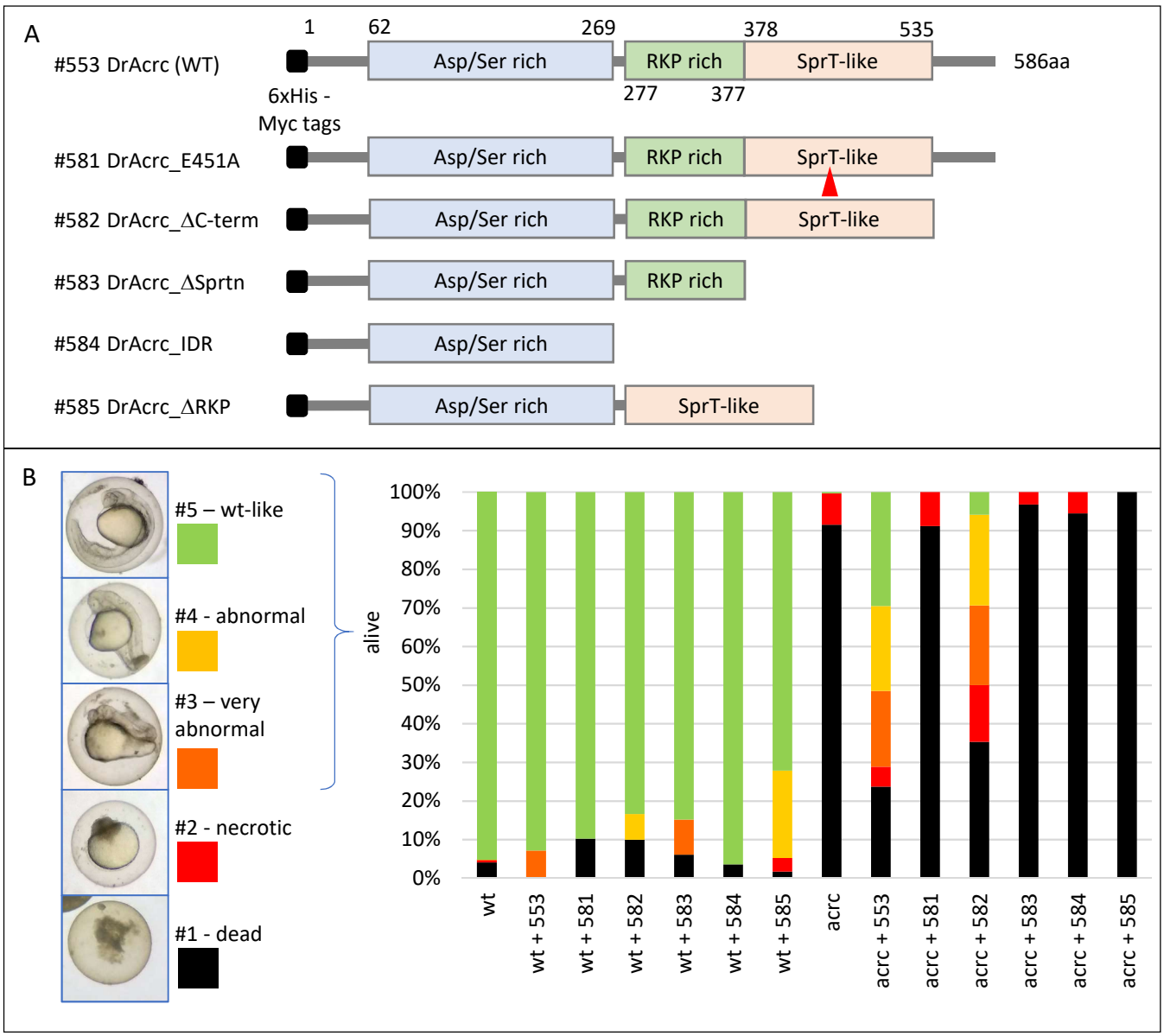

Figure 5. WT Acrc mRNA injections fully rescue the *acrc* maternal mutant phenotype. A – scheme of the injected rescue constructs: #553: DrAcrc-WT, #581: DrAcrc-E451A, #582: DrAcrc-ΔCterm, #583: DrAcrc-ΔSprtn, #584: DrAcrc-IDR, #585: DrAcrc-ΔRKP. B – phenotype characterization of rescued embryos with representative pictures. Wt and *acrc*$^{rbi5/rbi5}$ maternal mutant embryos were injected with 1nl of 250ng/ul RNA derived from the rescue constructs described above. Phenotypes were scored at 1dpf and divided into 5 categories: #1: dead, #2: necrotic, #3: very abnormal, #4: abnormal, #5: wt-like. Embryos in categories #3, 4 and 5 were considered alive. For detailed results, see Supplemental Table 1. Data shown are means.

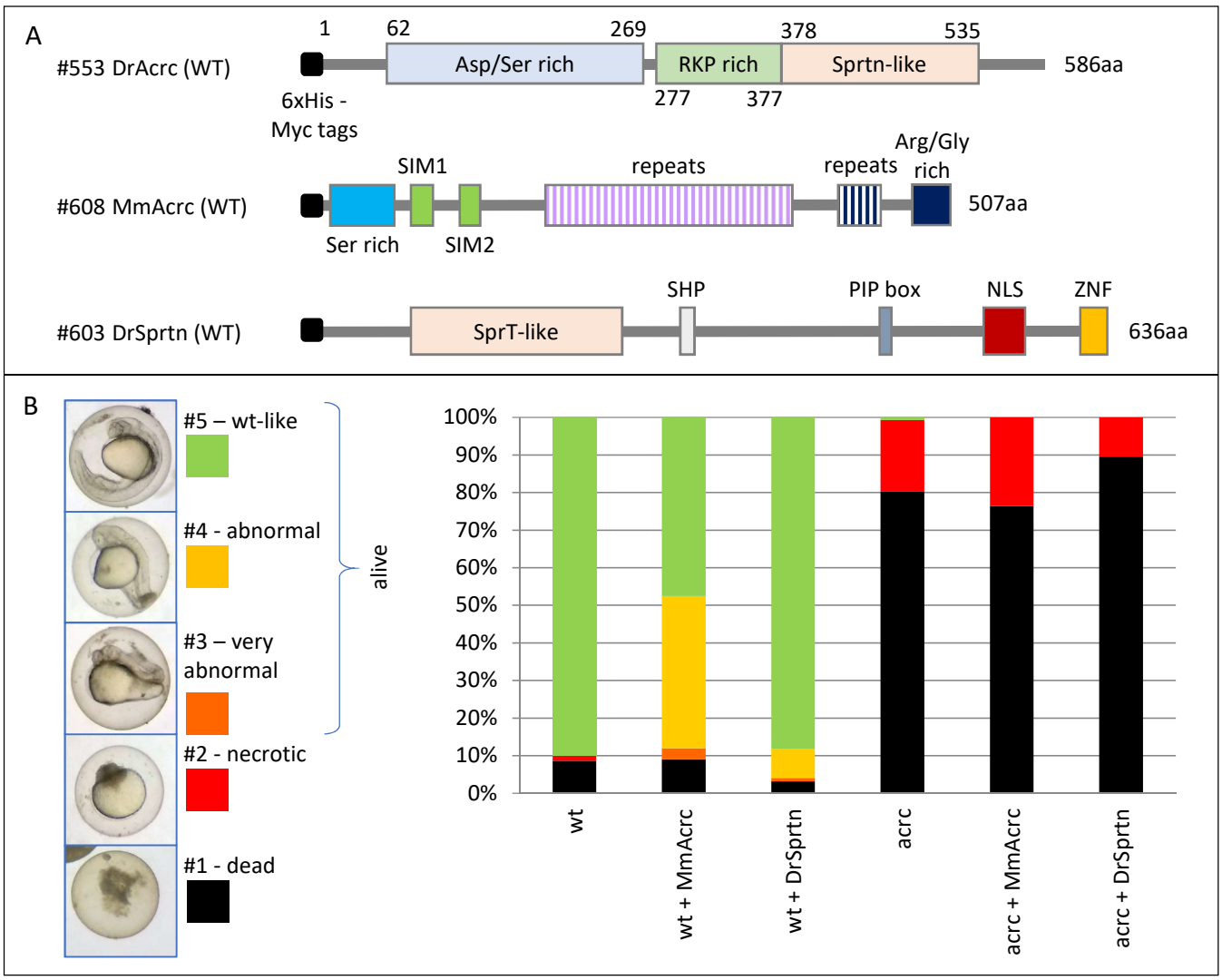

Figure 6. DrSprtn and MmAcrc mRNA injections do not rescue the *acrc* mutant phenotype. A – scheme of the injected rescue constructs: #608: MmAcrc, #603: DrSprtn. B – phenotype characterization of rescued embryos with representative pictures. Wt and *acrc*$^{rbi5/rbi5}$ maternal mutant embryos were injected with 1nl of 250ng/ul RNA derived from the rescue constructs described above. Phenotypes were scored at 1dpf and divided into 5 categories: #1: dead, #2: necrotic, #3: very abnormal, #4: abnormal, #5: wt-like. Embryos in categories #3, 4 and 5 were considered alive. For detailed results, see Supplemental Table 4. Data shown are means.

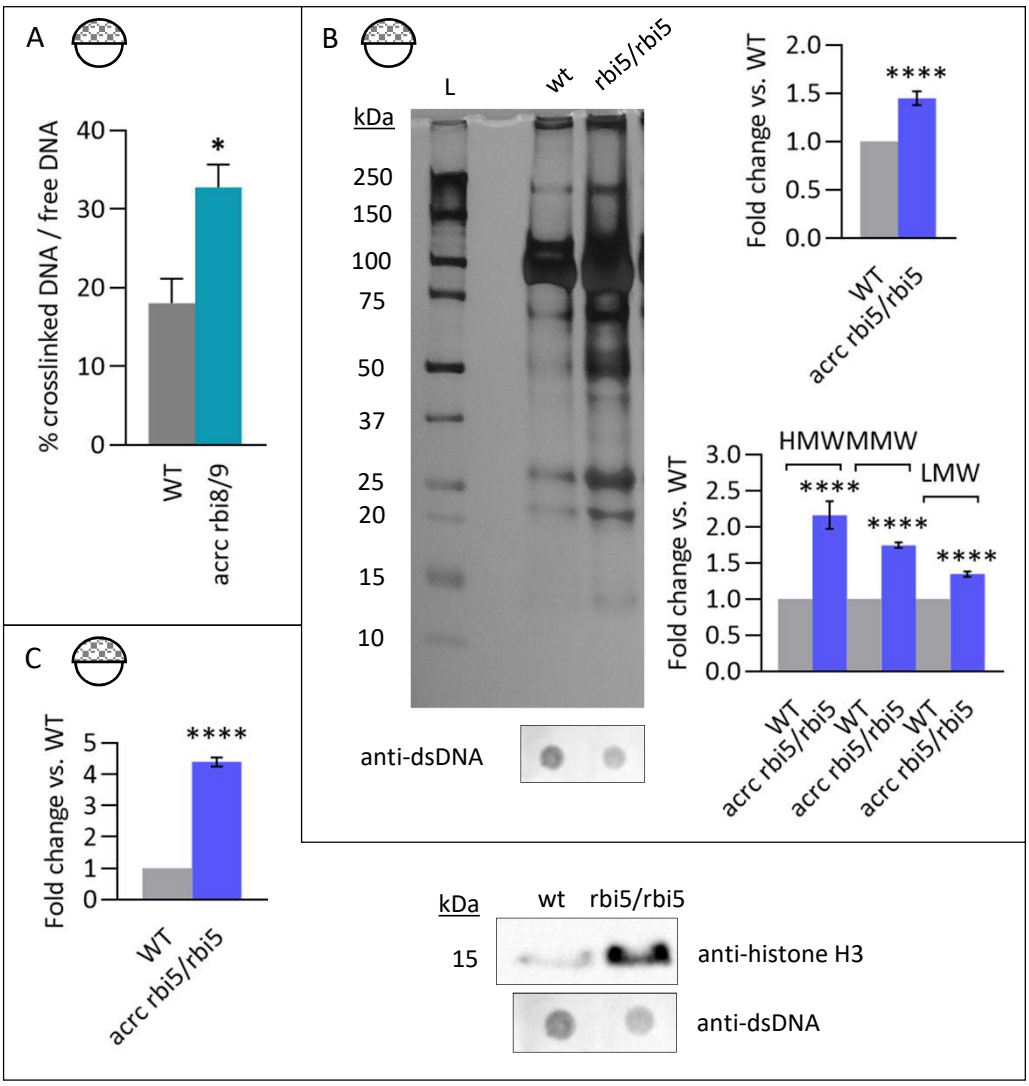

Figure 7. DPC measurements in 6 hpf zebrafish *acrc* mutant embryos. A – Total DPC levels (percentage of DNA-protein crosslinks vs. free DNA) as quantified using the KCl/SDS method: increased DPC levels in *acrc*$^{rbi8/9}$ maternal mutants relative to wt. An unpaired Student's t-test was performed for 3 biological replicates, pools of 100 embryos each (***: p-value = 0,0254). B-C – RADAR assays on 6 hpf embryos. Unpaired Student's t-test were performed for 4 biological replicates, pools of 50 embryos each (****: p-value < 0,0001). B – Total DPCs were isolated from n = 50 embryos each for WT and *acrc*$^{rbi5/rbi5}$ homozygotes, resolved on an SDS acrylamide gel, and stained with silver. Dot-blots showing DNA loading controls for DPC analysis prior to benzonase treatment are shown below; a DPC equivalent of 50 ng total DNA was loaded per well. C – Quantifications of total DPC staining intensities normalized to wt (top), and of staining intensities for high, middle and low molecular weight DPCs (bottom) based on data shown here and in Supplemental Figure S9A (4 biological replicates). D – Histone H3-DPC detection by western blot, with corresponding dot blot for dsDNA as loading control; a DPC equivalent of 50 ng total DNA was loaded per well. Total DPCs were isolated from 6-hpf old embryos, separated by SDS-PAGE and detected with H3-specific antibody. Quantification normalized to wt based on data shown here and in Supplemental Figure S9B (5 biological replicates). An unpaired Student's t-test was performed for 3 biological replicates, pools of 50 embryos each (****: p-value < 0,0001). L = ladder. Data shown are means with S.E.M.

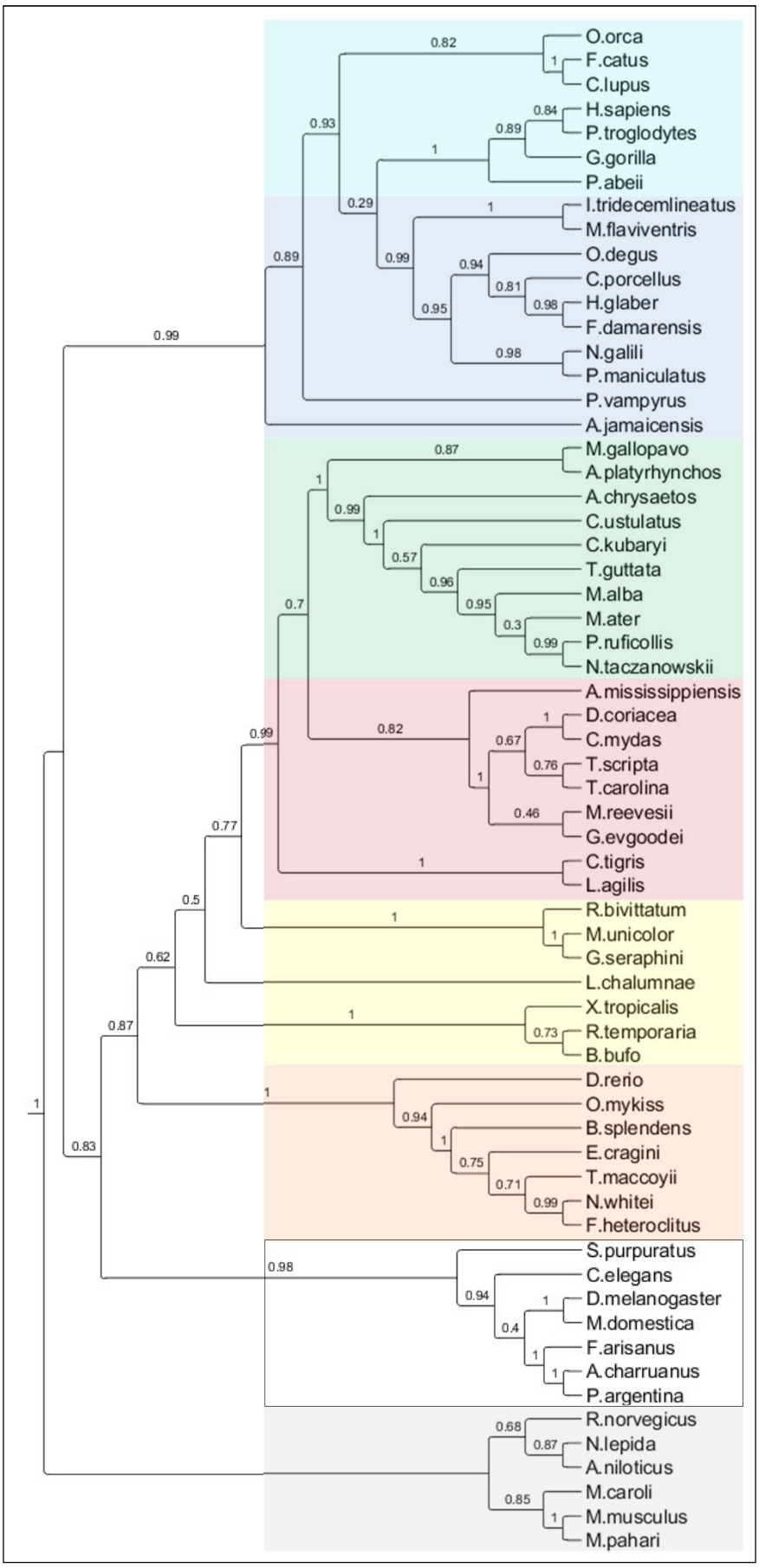

Supplemental Figure S1. Extended phylogenetic tree of ACRC/GCNA orthologs. Full-length protein sequences were aligned using MAFFT and the phylogenetic tree was constructed in PhyML. Blue: non-rodents mammals, dark blue: rodents and bats with a SprT-like domain, grey: rodents without SprT-like domain, green: birds, red: reptiles, yellow: amphibians, orange: fish, colorless: invertebrates.

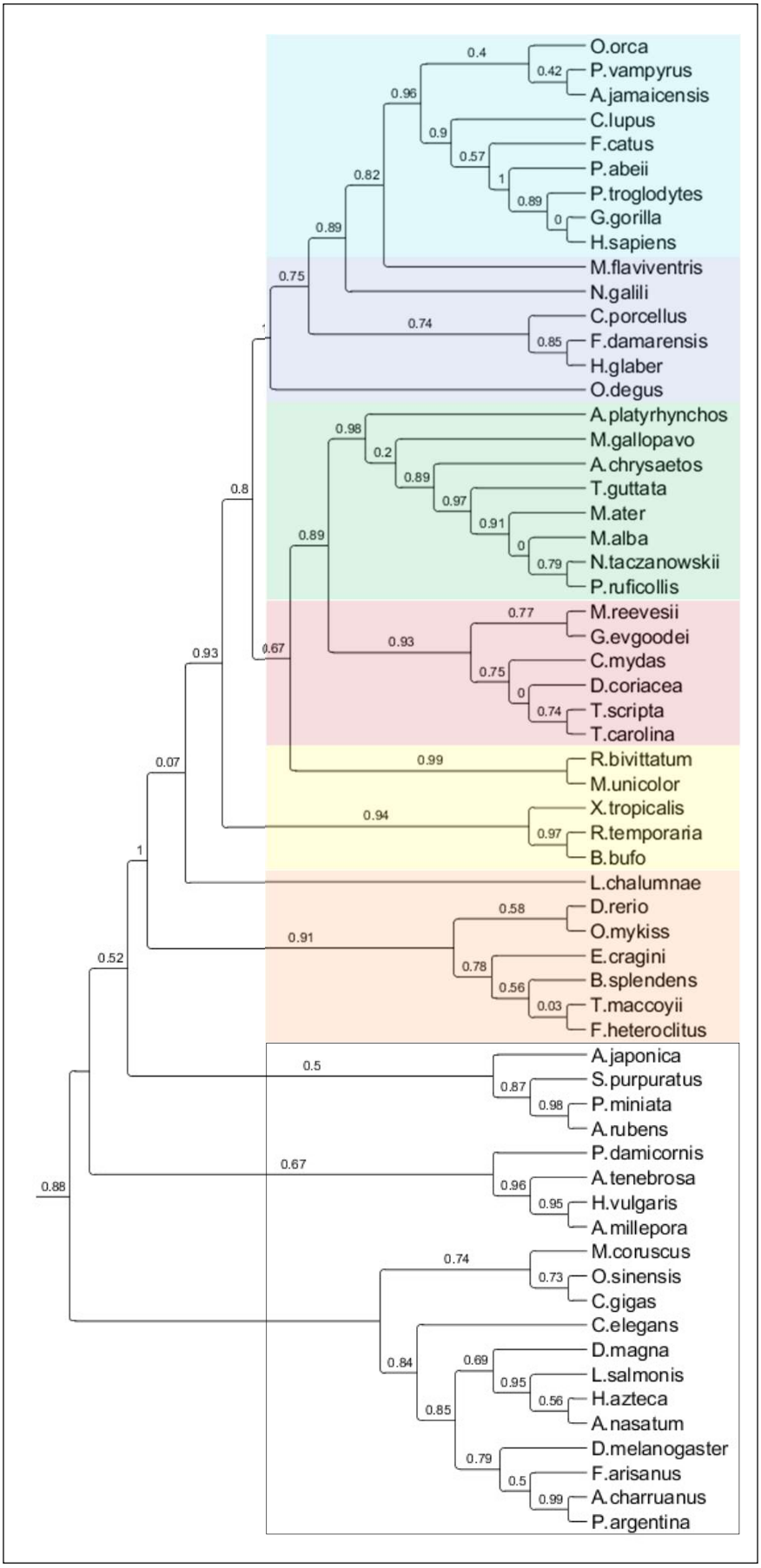

Supplemental Figure S2. Extended phylogenetic tree of ACRC/GCNA orthologs. SprtT-like domains protein sequences were aligned using MAFFT and the phylogenetic tree was constructed in PhyML. Blue: non-rodents mammals, dark blue: rodents with a SprT-like domain, green: birds, red: reptiles, yellow: amphibians, orange: fish, colorless: invertebrates.

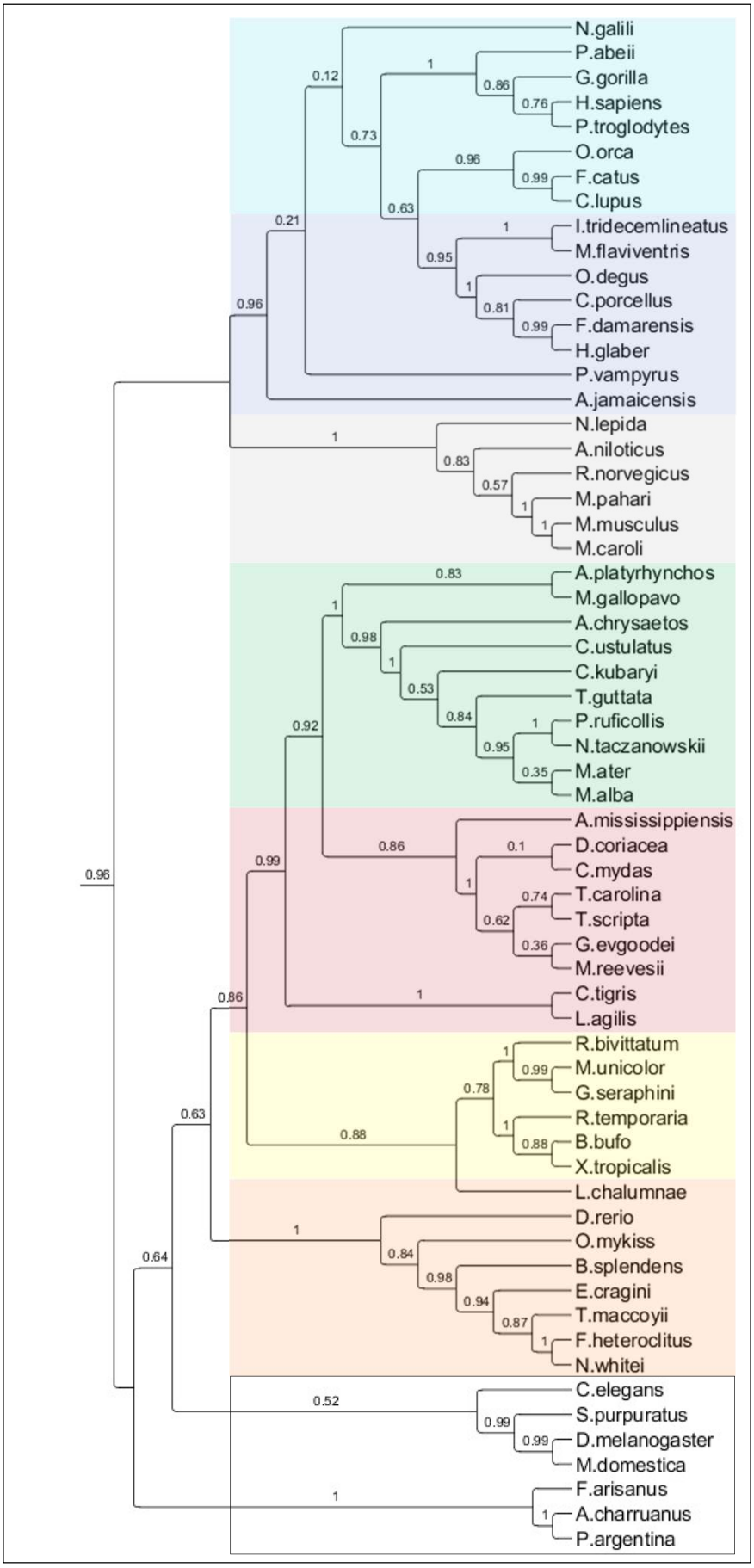

Supplemental Figure S3. Extended phylogenetic tree of ACRC/GCNA orthologs. N domain/non-structured N half protein sequences were aligned using MAFFT and the phylogenetic tree was constructed in PhyML. Blue: non-rodents mammals, dark blue: rodents and bats with a SprT-like domain, grey: rodents without SprT-like domain, green: birds, red: reptiles, yellow: amphibians, orange: fish, colorless: invertebrates.

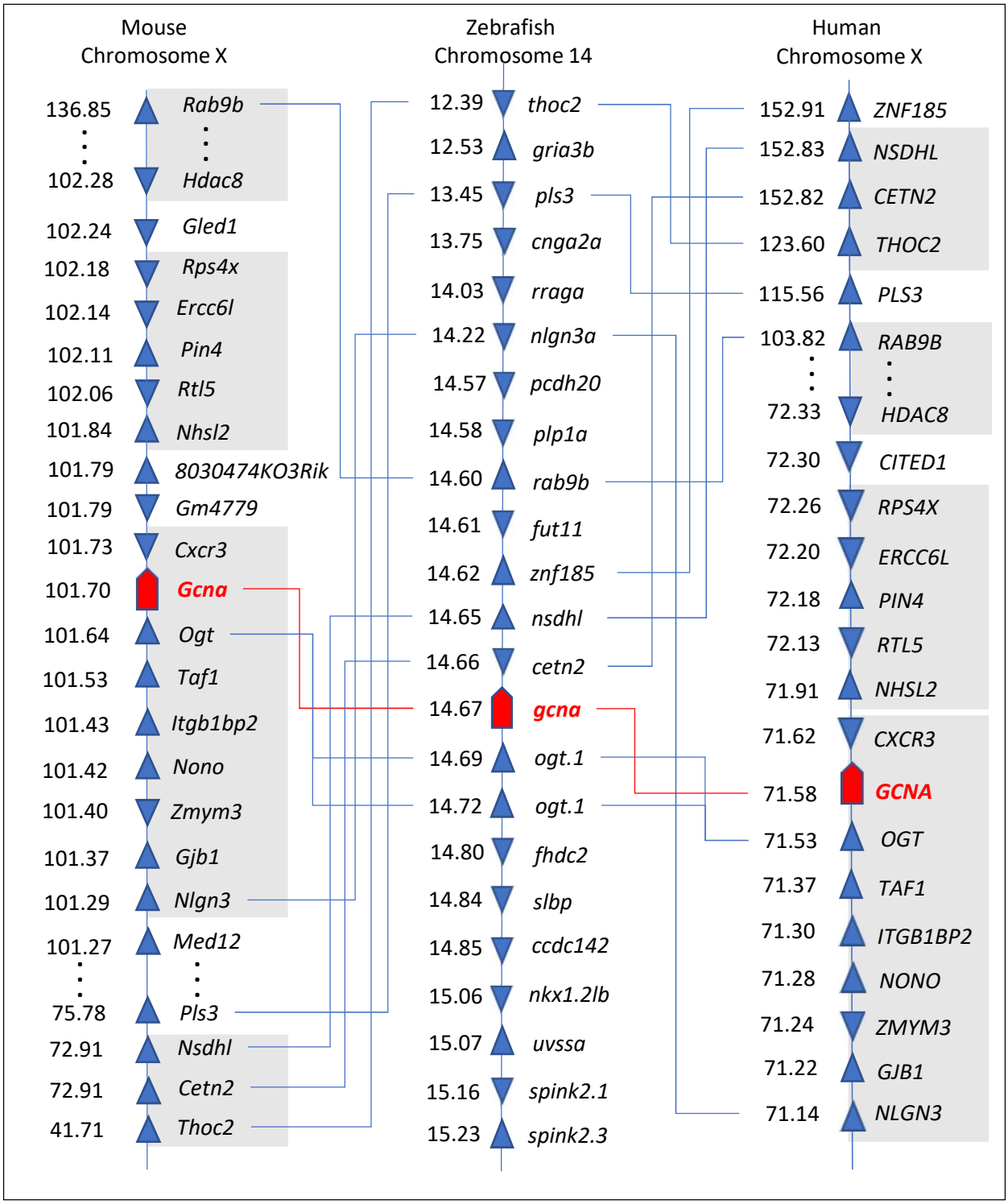

Supplemental Figure S4. Conserved synteny analysis of zebrafish, mouse and human ACRC/GCNA genes. Numbers next to the gene names represent megabase pair (Mbp) of gene location on the chromosome. Chromosome segments are represented with blue (continuous segments). Orthologs are connected with lines. Grey background highlights regions with conserved gene order between mouse and human.

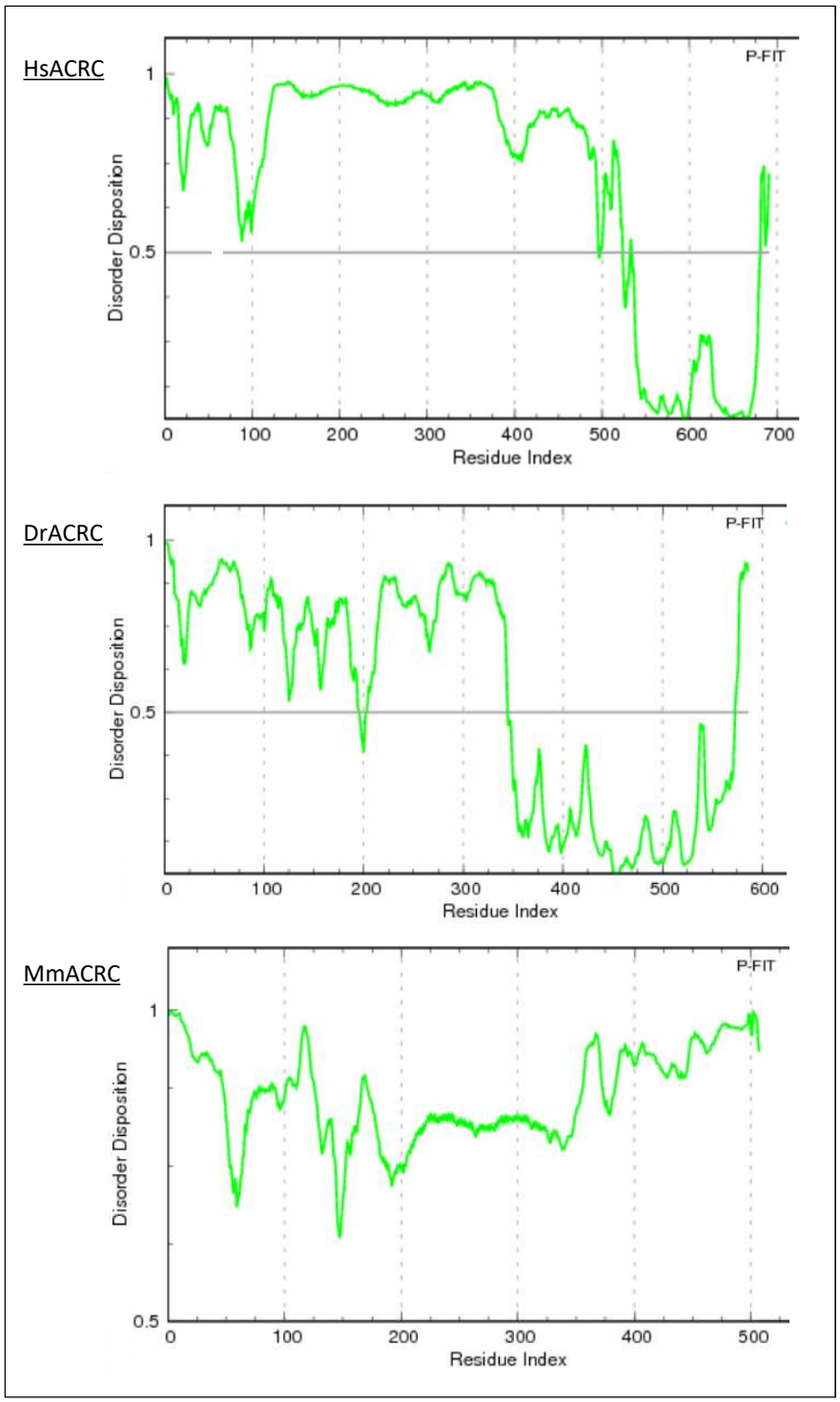

Supplemental Figure S5. Disorder disposition plot for human, zebrafish and mouse ACRC predicted using PONDR-FIT workspace. Values above 0.5. indicate disordered regions.

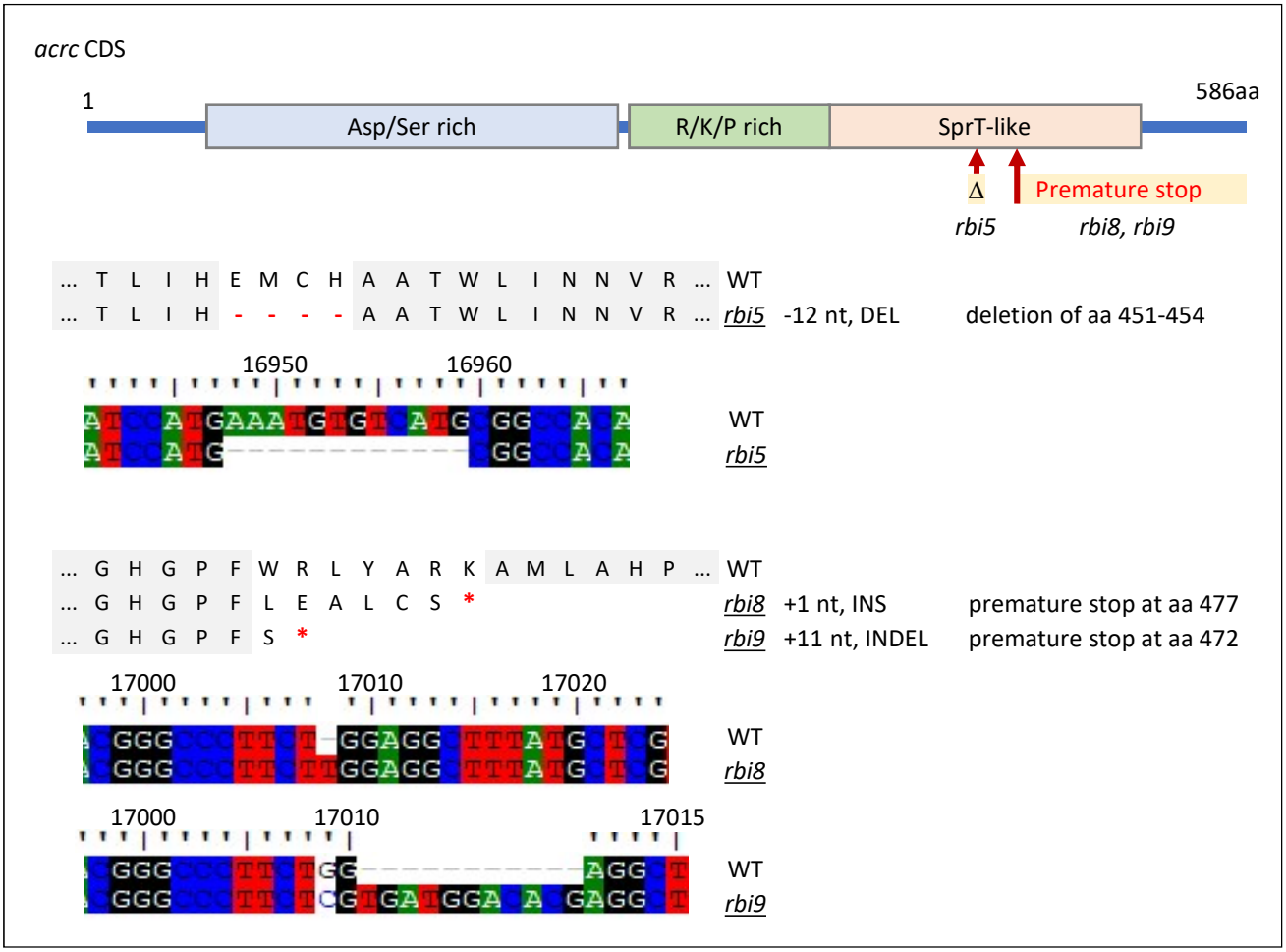

Supplemental Figure S6. Creation of two *acrc* mutant zebrafish strains. Scheme of the deleted domains in *acrc* mutant alleles *rbi5* and *rbi8* & *rbi9*. *rbi5* allele: the deletion of 12 basepairs leads to a 4 amino-acids deletion (ΔEMCH, aa 451-454) in the enzymatic core of the SprT-like domain of Acrc; *rbi8* allele: the insertion of 1 basepair leads to a premature stop codon at aa 477; *rbi9* allele: the indel of 11 basepairs leads to a premature stop codon at aa 472. Both *rbi8* and *rbi9* alleles result in a truncation of the C-terminus of Acrc, including half of the Sprtn domain. All 3 alleles were created using CrispR/Cas9 technology.

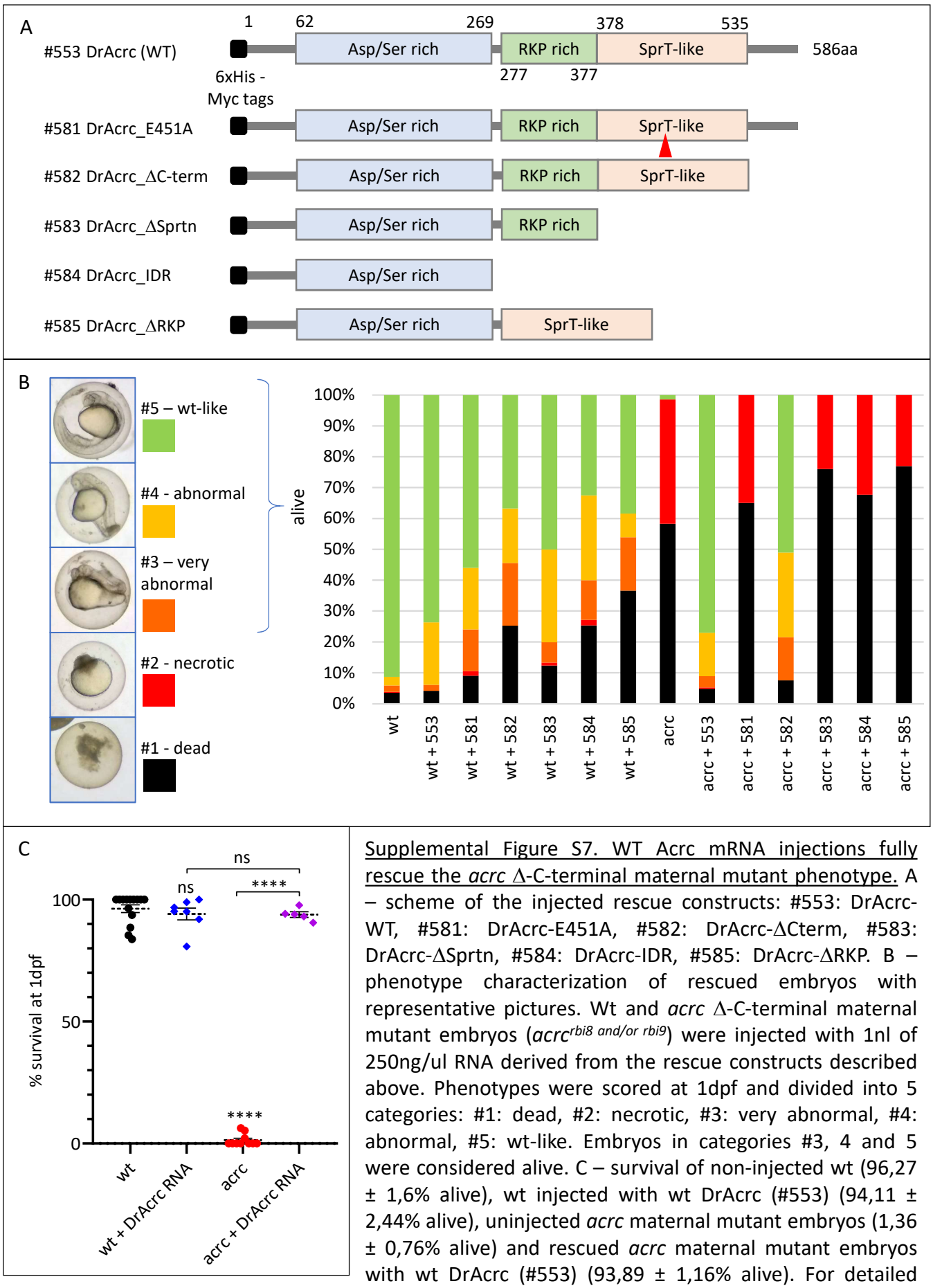

Supplemental Figure S7. WT Acrc mRNA injections fully rescue the *acrc* Δ-C-terminal maternal mutant phenotype. A – scheme of the injected rescue constructs: #553: DrAcrc-WT, #581: DrAcrc-E451A, #582: DrAcrc-ΔCterm, #583: DrAcrc-ΔSprtn, #584: DrAcrc-IDR, #585: DrAcrc-ΔRKP. B – phenotype characterization of rescued embryos with representative pictures. Wt and *acrc* Δ-C-terminal maternal mutant embryos (*acrc*$^{rbi8\ and/or\ rbi9}$) were injected with 1nl of 250ng/ul RNA derived from the rescue constructs described above. Phenotypes were scored at 1dpf and divided into 5 categories: #1: dead, #2: necrotic, #3: very abnormal, #4: abnormal, #5: wt-like. Embryos in categories #3, 4 and 5 were considered alive. C – survival of non-injected wt (96,27 ± 1,6% alive), wt injected with wt DrAcrc (#553) (94,11 ± 2,44% alive), uninjected *acrc* maternal mutant embryos (1,36 ± 0,76% alive) and rescued *acrc* maternal mutant embryos with wt DrAcrc (#553) (93,89 ± 1,16% alive). For detailed results, see Supplemental Table 3. Data shown are means.

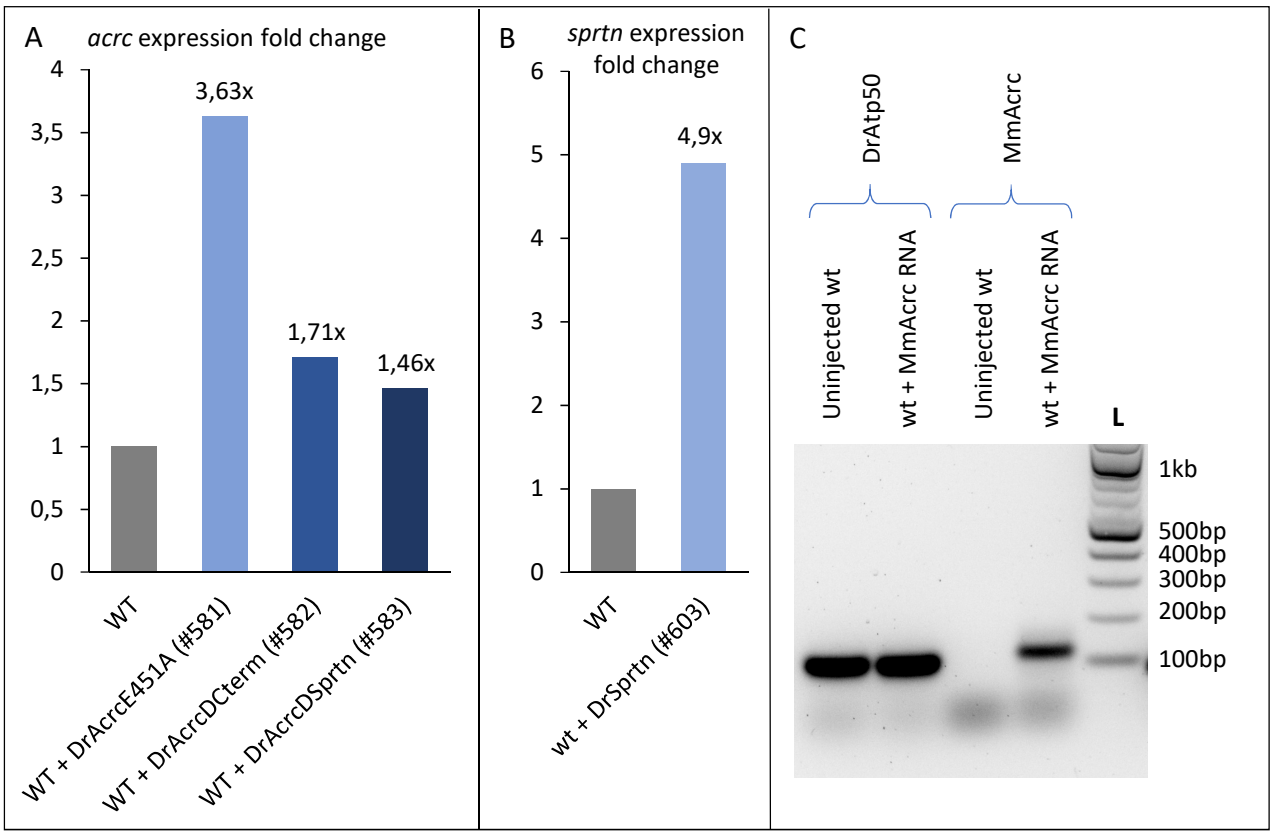

Supplemental Figure S8. mRNAs expressed from the rescue constructs are enriched in WT. A - RT-qPCR results showing the upregulation of zebrafish *acrc* in wt embryos injected with the following DrAcrc rescue constructs at 2dpf relative to uninjected wt: DrAcrcE451A (#581), DrAcrcΔCterm (#582), DrAcrcΔSprtn (#583). DrSprtn expression was normalized to Dr18S. The cDNAs were obtained from 1 pool of 20 embryos for each sample. B - RT-qPCR results showing the upregulation of zebrafish *sprtn* in wt embryos injected with the DrSprtn rescue construct (#603) at 1dpf relative to uninjected wt. DrSprtn expression was normalized to Dr18S. The cDNAs were obtained from 1 pool of 5 embryos for each sample. C – PCR products of *Atp50* amplification (as housekeeping gene, 93bp) and of mouse *Acrc* amplification (107bp) on cDNA derived from 2dpf non-injected wt and wt injected with RNA from rescue construct #608 encoding full-length mouse Acrc cds (1 pool of 20 embryos each). L = DNA ladder.

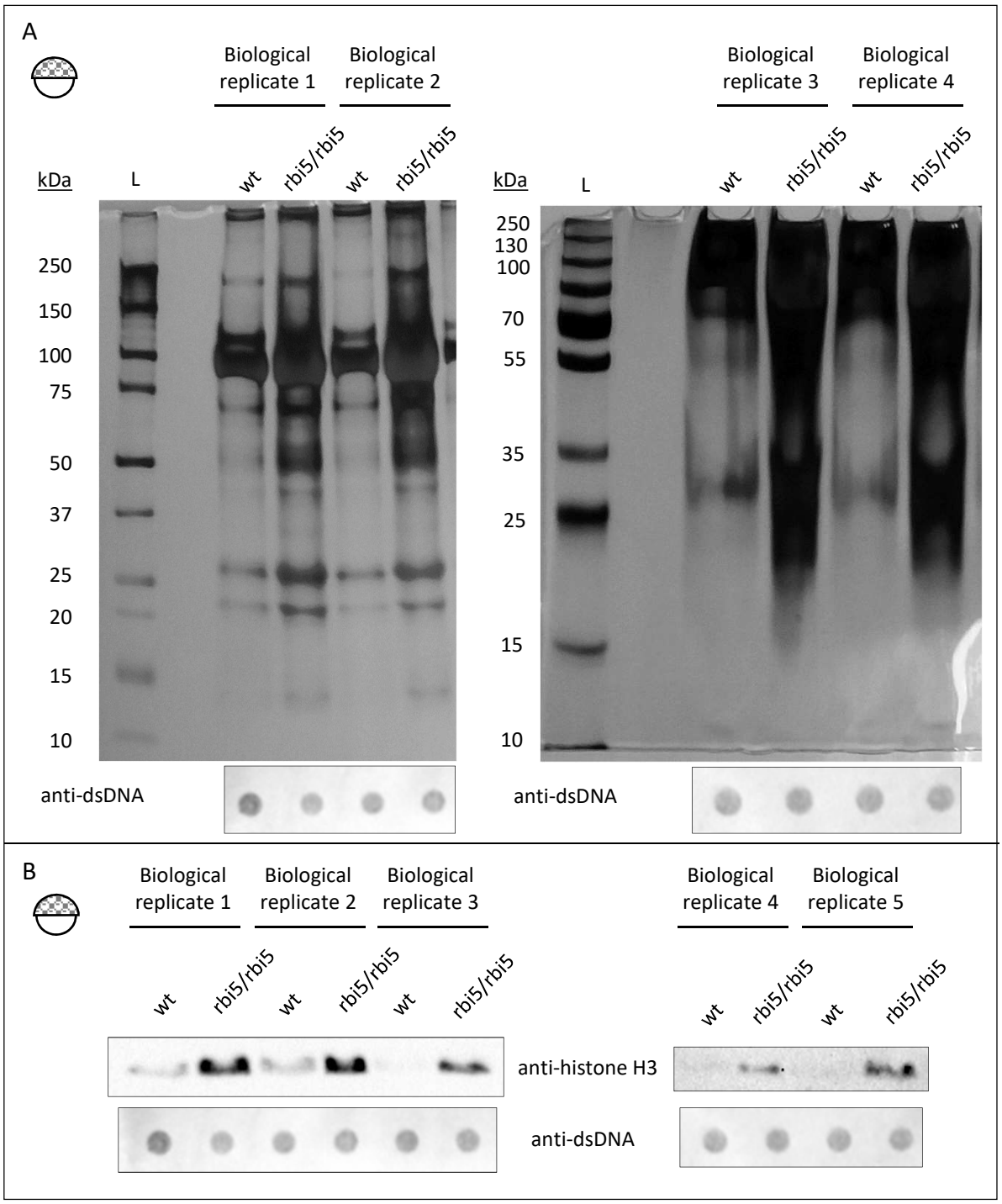

Supplemental Figure S9. DPC measurements in 6 hpf zebrafish *acrc* mutant embryos by RADAR. A – Total DPCs isolated from wt and *acrc*$^{rbi5/rbi5}$ homozygous maternal mutants were separated on an SDS acrylamide gel and stained with silver. Dot blots beneath show equal dsDNA loading; the equivalent of 50 ng of DNA was loaded per well. Shown are 4 biological replicates whose quantification is shown in Figure 7B. B – Histone 3 DPC detection by western blot, with dot blot for dsDNA. Shown are 5 biological replicates whose quantification is shown in Figure 7C. L = ladder.

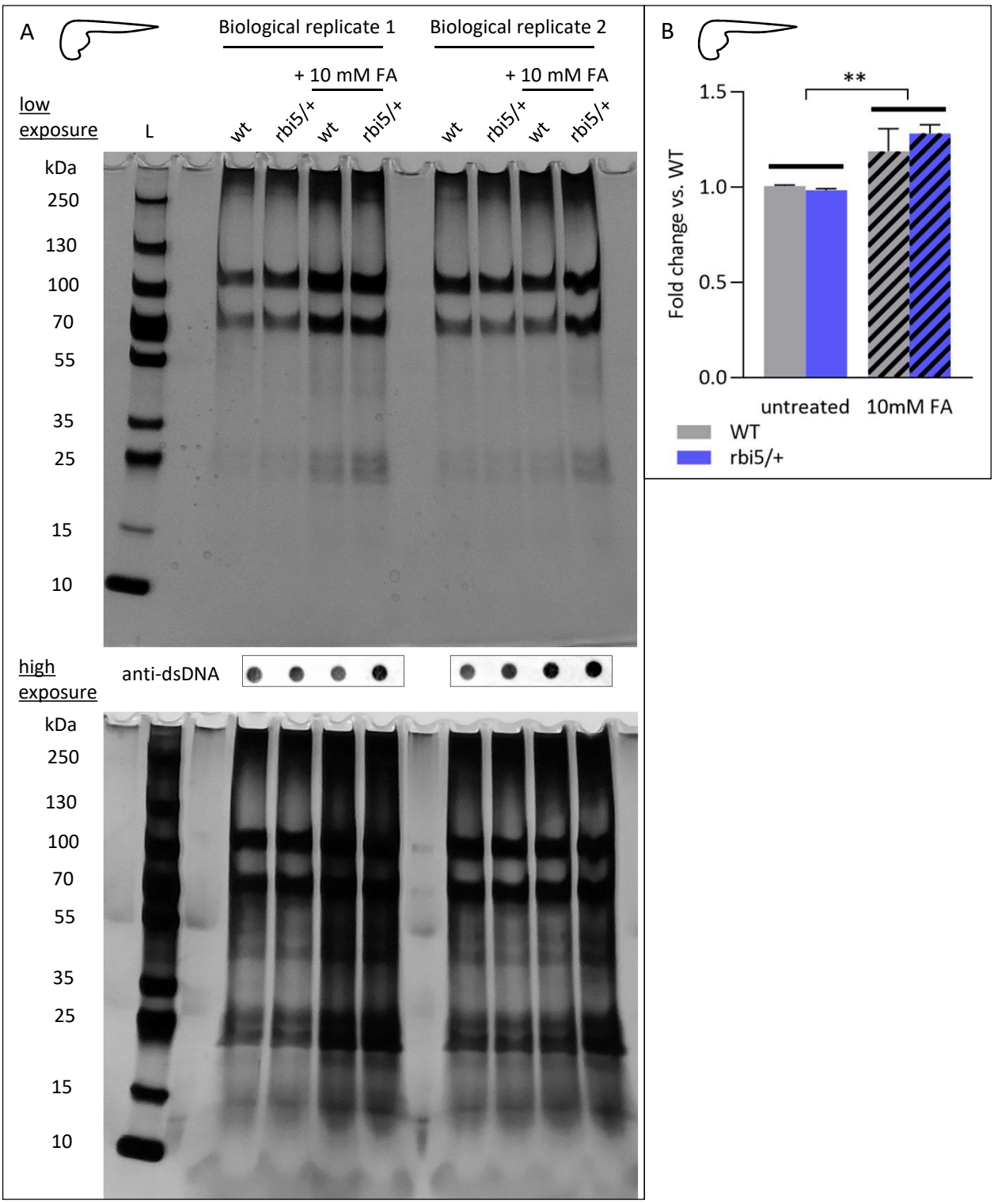

Supplemental Figure S10. DPC measurements in zebrafish embryos with reduced Acrc levels. RADAR assays followed by SDS acrylamide gel separation and silver staining of DPCs from 2 dpf wt and *rbi5* heterozygous embryos treated or not with 10 mM FA for 30 minutes. Shown are biological duplicates, with low exposure (top) and high exposure (bottom). Quantifications of the staining intensities normalized to wt are shown in B. Dot blot for dsDNA shows equal loading; total DPCs were normalized to DNA and an equivalent of 150 ng of DNA was loaded per well. A two-way ANOVA analysis was performed, followed by Tukey's multiple comparisons test; **: p-value = 0,0022. L = ladder. Data shown are means with S.E.M.

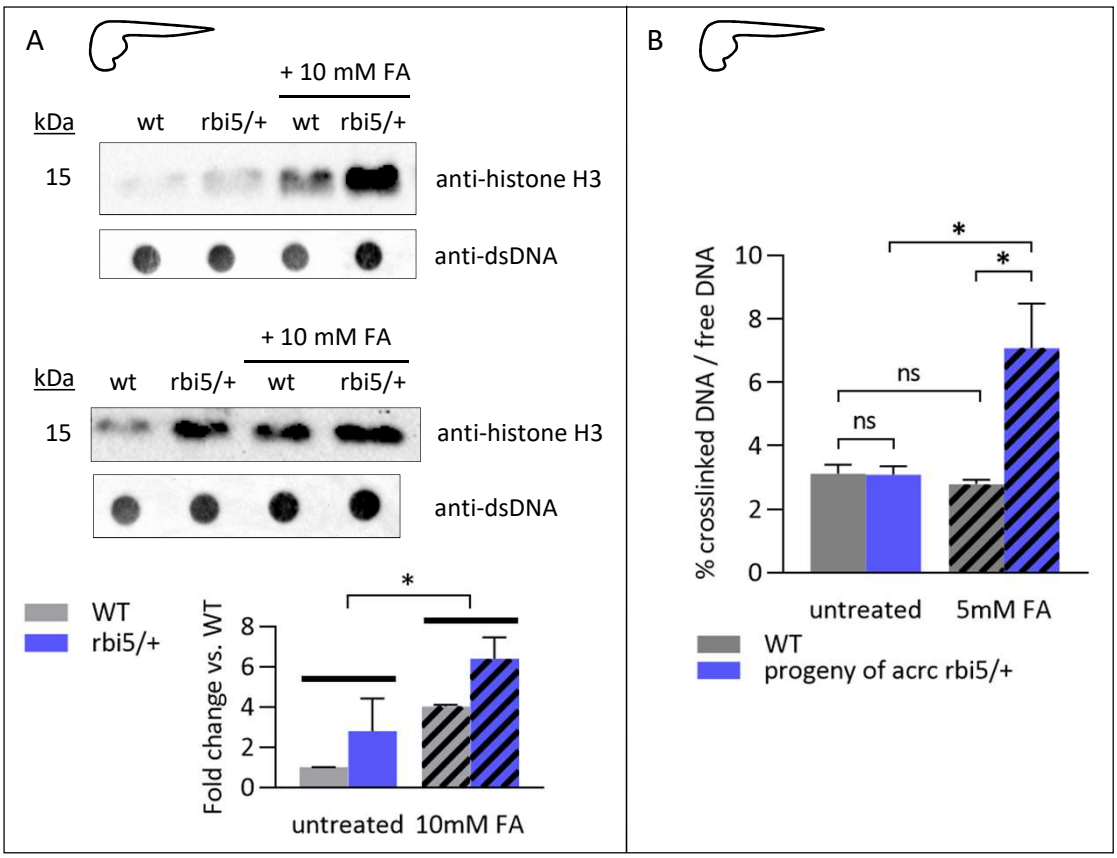

Supplemental Figure S11. DPC measurements in zebrafish embryos with reduced Acrc levels. A – RADAR assays followed by histone H3 DPC detection by western blot, with dot blot for dsDNA as a loading control (the equivalent of 150 ng of DNA was loaded per well). Shown are 2 biological duplicates and the quantification of H3 staining intensities normalized to wt. RADAR performed on 2 dpf wt and *rbi5* heterozygous embryos treated or not with 10 mM FA for 30 minutes. A two-way ANOVA analysis was performed, followed by Tukey's multiple comparisons test; *: p-value = 0,0277. B – Total DPC levels (percentage of DNA-protein crosslinks vs. free DNA) as quantified using the KCl/SDS method. DPC levels quantified in 3dpf embryos after exposure to 5 mM formaldehyde (FA) for 1 hour. Acrc samples consist in the progeny of incrossed heterozygous *acrc*$^{rbi5/+}$ parents: 25% wt, 50% heterozygotes and 25% mutants; all embryos are viable due to maternal Acrc deposition in the eggs. Two-way ANOVA analysis followed by Tukey's multiple comparisons tests were performed for 3 biological replicates, pools of 10 embryos each; *: p-value < 0,05. L = ladder. Data shown are means with S.E.M. Ns = not significant.